Article

Cell Metabolism

# Extracellular Vesicle-Contained eNAMPT Delays Aging and Extends Lifespan in Mice

## Graphical Abstract

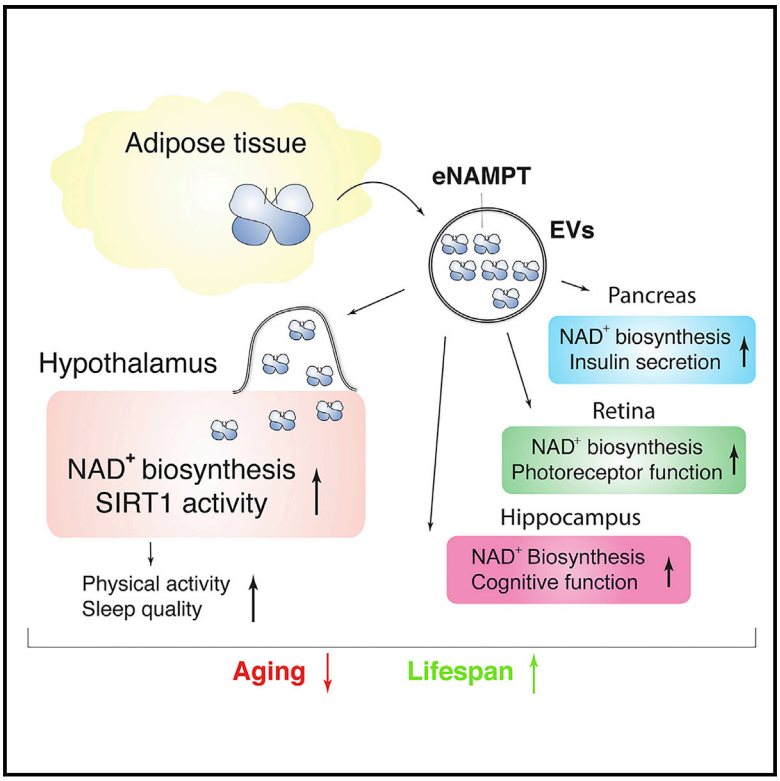


## Highlights

- Circulating levels of eNAMPT decline with age in both mice and humans
- Increasing eNAMPT promotes $NAD^+$, counteracts aging, and extends healthspan in mice
- eNAMPT is contained exclusively in extracellular vesicles (EVs) in mice and humans
- Supplementing eNAMPT in EVs improves physical activity and extends lifespan in mice

## Authors

Mitsukuni Yoshida, Akiko Satoh, Jonathan B. Lin, ..., Michael Wong, Rajendra S. Apte, Shin-ichiro Imai

## Correspondence

imaishin@wustl.edu

## In Brief

Yoshida et al. demonstrate that the levels of extracellular nicotinamide phosphoribosyltransferase (eNAMPT) decline with age in mice and humans. Increasing eNAMPT promotes $NAD^+$, counteracting aging and extending healthspan. eNAMPT is contained in extracellular vesicles (EVs). Supplementing eNAMPT-containing EVs improves physical activity and extends mouse lifespan, suggesting a potential anti-aging intervention.

Yoshida et al., 2019, Cell Metabolism *30*, 1–14
August 6, 2019 
https://doi.org/10.1016/j.cmet.2019.05.015

CellPress

Please cite this article in press as: Yoshida et al., Extracellular Vesicle-Contained eNAMPT Delays Aging and Extends Lifespan in Mice, Cell Metabolism (2019), https://doi.org/10.1016/j.cmet.2019.05.015

Cell Metabolism
Article



# Extracellular Vesicle-Contained eNAMPT Delays Aging and Extends Lifespan in Mice

Mitsukuni Yoshida,[1,6] Akiko Satoh,[7] Jonathan B. Lin,[2,6] Kathryn F. Mills,[1] Yo Sasaki,[3] Nicholas Rensing,[4] Michael Wong,[4] Rajendra S. Apte,[1,2,5] and Shin-ichiro Imai[1,5,8,9,*]

[1]Department of Developmental Biology, Washington University School of Medicine, St. Louis, MO 63110, USA
[2]Department of Ophthalmology & Visual Sciences, Washington University School of Medicine, St. Louis, MO 63110, USA
[3]Department of Genetics, Washington University School of Medicine, St. Louis, MO 63110, USA
[4]Department of Neurology, Washington University School of Medicine, St. Louis, MO 63110, USA
[5]Department of Medicine, Washington University School of Medicine, St. Louis, MO 63110, USA
[6]MD-PhD Program, Washington University School of Medicine, St. Louis, MO 63110, USA
[7]Sleep and Aging Research Regulation Project Team, National Center for Geriatrics and Gerontology, Aichi, Japan
[8]Department of Gerontology, Laboratory of Molecular Life Science, Institute of Biomedical Research and Innovation, Kobe, Japan
[9]Lead Contact
*Correspondence: imaishin@wustl.edu
https://doi.org/10.1016/j.cmet.2019.05.015

## SUMMARY

**Aging is a significant risk factor for impaired tissue functions and chronic diseases. Age-associated decline in systemic $NAD^+$ availability plays a critical role in regulating the aging process across many species. Here, we show that the circulating levels of extracellular nicotinamide phosphoribosyltransferase (eNAMPT) significantly decline with age in mice and humans. Increasing circulating eNAMPT levels in aged mice by adipose-tissue-specific overexpression of NAMPT increases $NAD^+$ levels in multiple tissues, thereby enhancing their functions and extending healthspan in female mice. Interestingly, eNAMPT is carried in extracellular vesicles (EVs) through systemic circulation in mice and humans. EV-contained eNAMPT is internalized into cells and enhances $NAD^+$ biosynthesis. Supplementing eNAMPT-containing EVs isolated from young mice significantly improves wheel-running activity and extends lifespan in aged mice. Our findings have revealed a novel EV-mediated delivery mechanism for eNAMPT, which promotes systemic $NAD^+$ biosynthesis and counteracts aging, suggesting a potential avenue for anti-aging intervention in humans.**

## INTRODUCTION

In recent years, nicotinamide adenine dinucleotide ($NAD^+$) metabolism has emerged as a central topic in the field of aging and longevity research (Cantó et al., 2015; Rajman et al., 2018; Verdin, 2015; Yoshino et al., 2018). It has now been established that $NAD^+$ availability declines over age at a systemic level, triggering a variety of age-associated pathophysiological changes in diverse model organisms. In mammals, the age-associated decline in $NAD^+$ availability appears to be caused by two major events: decreased $NAD^+$ biosynthesis and increased $NAD^+$ consumption (Imai, 2016; Imai and Guarente, 2014). The former could be caused by chronic inflammation with enhanced oxidative stress and/or increased inflammatory cytokines, whereas the latter could be caused by increased DNA damage. As a consequence, $NAD^+$ levels decrease with age in multiple tissues, including adipose tissue, skeletal muscle, liver, pancreas, skin, neurosensory retina, and brain (Cantó et al., 2015; Lin et al., 2018; Rajman et al., 2018; Verdin, 2015; Yoshino et al., 2018). The realization of such systemic $NAD^+$ decline as a fundamental event for age-associated pathophysiology has now provided a strong rationale to develop effective anti-aging interventions using key $NAD^+$ intermediates, such as nicotinamide mononucleotide (NMN) and nicotinamide riboside (NR) (Rajman et al., 2018; Yoshino et al., 2018). Indeed, many studies have already proven the efficacy of NMN and NR to mitigate age-associated functional decline and treat age-associated disease conditions in various mouse models (Rajman et al., 2018; Yoshino et al., 2018).

### Context and Significance

The availability of $NAD^+$, an essential chemical for energy metabolism in all living organisms, declines over age, causing age-associated problems. It remains unclear what contributes to systemic $NAD^+$ regulation. Yoshida et al. demonstrate that the circulating levels of extracellular nicotinamide phosphoribosyltransferase (eNAMPT), a key $NAD^+$ biosynthetic enzyme in mammals, decline with age in mice and humans. Increasing eNAMPT promotes $NAD^+$ in tissues, enhancing their functions and extending healthspan. eNAMPT is carried in small particles called extracellular vesicles (EVs). Supplementing eNAMPT-containing EVs improves physical activity and extends lifespan in mice, revealing a novel mechanism by which eNAMPT regulates systemic $NAD^+$ biosynthesis and counteracts aging and implicating an anti-aging intervention in humans.

In mammals, nicotinamide phosphoribosyltransferase (NAMPT) is the rate-limiting enzyme in a major $NAD^+$ biosynthetic pathway, converting nicotinamide and 5′-phosphoribosyl-pyrophosphate (PRPP) to NMN (Garten et al., 2015; Imai, 2009). Interestingly, there are two distinct forms of NAMPT in mammals: intra- and extracellular NAMPT (iNAMPT and eNAMPT, respectively) (Revollo et al., 2007). Whereas the function of iNAMPT as a critical $NAD^+$ biosynthetic enzyme has been fully established, the physiological relevance and function of eNAMPT has long been controversial. eNAMPT was previously identified as pre-B cell colony-enhancing factor (PBEF) and insulin-mimetic visfatin, neither of which has been reconfirmed to date (Fukuhara et al., 2007; Garten et al., 2015; Imai, 2009; Samal et al., 1994). Additionally, eNAMPT was also reported to function as a proinflammatory cytokine, although this particular function has not yet been confirmed in loss- or gain-of-function *Nampt* mutants (Dahl et al., 2012). We have previously demonstrated the physiological relevance of eNAMPT *in vivo* by adipose-tissue-specific genetic manipulation of *Nampt* (Yoon et al., 2015). Adipose-tissue-specific *Nampt* knockout (ANKO) mice, particularly females, show significant decreases in circulating eNAMPT levels. Surprisingly, ANKO mice exhibit a significant reduction in $NAD^+$ levels not only in adipose tissue, but also in other remote tissues such as the hypothalamus (Yoon et al., 2015). Subsequent intensive investigations have revealed a novel function of eNAMPT that enhances $NAD^+$, SIRT1 activity, and neural activation in the hypothalamus in response to fasting. These findings suggest the existence of a novel intertissue communication system between adipose tissue and the hypothalamus, mediated by eNAMPT (Imai, 2016). However, how exactly eNAMPT regulates hypothalamic $NAD^+$ levels has remained elusive.

Because the hypothalamus has been suggested to function as a high-order control center of aging in mammals (Satoh et al., 2013; Zhang et al., 2013, 2017), we hypothesized that eNAMPT secreted from adipose tissue plays a critical role in affecting the process of aging and eventually lifespan. To address this hypothesis, we generated adipose-tissue-specific *Nampt* knockin (ANKI) mice (Yoon et al., 2015) and characterized their aging phenotypes. Interestingly, aged ANKI mice maintained youthful levels of circulating eNAMPT and increased $NAD^+$ levels in multiple tissues including the hypothalamus, hippocampus, pancreas, and retina, exhibiting significant improvement in physical activity, sleep quality, cognitive function, glucose metabolism, and photoreceptor functions. With these beneficial effects against aging, ANKI mice, particularly females, showed a significant extension of healthspan. Surprisingly, we found that eNAMPT was carried in extracellular vesicles (EVs) through blood circulation in mice and humans. EV-contained eNAMPT was internalized into primary hypothalamic neurons and enhanced $NAD^+$ biosynthesis intracellularly. Injecting eNAMPT-containing EVs purified from young mice or cultured adipocytes, but not from *Nampt*-knockdown adipocytes, was able to enhance wheel-running activity and extend lifespan in aged mice. These findings demonstrate a novel intertissue communication mechanism driven by an EV-mediated delivery of eNAMPT. This new physiological system mediated by EV-contained eNAMPT plays a critical role in maintaining systemic $NAD^+$ biosynthesis and counteracting age-associated physiological decline, implicating EV-contained eNAMPT as a potential anti-aging biologic in humans.

## RESULTS

### Plasma eNAMPT Levels Decline with Age in Both Mice and Humans

Our previous study has demonstrated that adipose NAMPT expression decreases with age (Yoshino et al., 2011). Consistently, we found that the protein expression levels of iNAMPT in isolated adipocytes decreased from 6 to 18 months of age (Figure S1A). Given that adipose tissue is a major source of circulating eNAMPT (Yoon et al., 2015), we examined whether circulating eNAMPT levels changed during aging in mice. Plasma eNAMPT levels significantly declined from 6 to 18 months of age by 33% and 74% in both female and male mice, respectively (Figure 1A). In young (6-month-old) mice, calculated plasma eNAMPT concentrations were higher in females (55–123 ng/μL) compared to those in males (29–52 ng/μL). However, in aged (18-month-old) mice, both males and females showed significant decline in circulating eNAMPT levels throughout a day (Figures 1B and S1B).

The age-associated reduction in plasma eNAMPT raised a possibility that plasma eNAMPT levels could be a valuable surrogate biomarker for aging. Thus, we measured plasma eNAMPT levels across several different age groups in mice and humans. We found that plasma eNAMPT levels linearly declined with age in both mice and humans (Figure 1C), suggesting that the process underlying eNAMPT secretion and its potential significance during aging might be conserved in both species. To further evaluate the potential association between plasma eNAMPT levels and aging, we asked whether the reduced levels of plasma eNAMPT could predict higher mortality risks and remaining lifespans of mice in a small prospective study. Intriguingly, the number of days for which an individual mouse lived since the day of eNAMPT measurement was highly correlated with their plasma eNAMPT levels (Figure 1D). The higher the level of plasma eNAMPT went, the longer the remaining lifespan became. These results led us to the interesting hypothesis that circulating eNAMPT might play a critical role in regulating not only the process of aging and but also lifespan in mammals.

### Adipose-Tissue-Specific Overexpression of *Nampt* Maintains Plasma eNAMPT Levels and $NAD^+$ Biosynthesis in Multiple Tissues during Aging

To investigate the role of eNAMPT in aging and longevity control, we examined aging cohorts of adipose-tissue-specific *Nampt* knock-in (ANKI) mice (Yoon et al., 2015). At 4 months of age, plasma eNAMPT levels did not differ between ANKI and control mice under an *ad libitum*-fed condition (Figure 2A). Young ANKI mice showed significantly higher levels of plasma eNAMPT only in response to fasting (Yoon et al., 2015). When they reached 24 months of age, plasma eNAMPT levels were maintained at 3.3- and 3.6-fold higher levels in ANKI female and male mice, respectively, compared to those in the age-matched control mice (Figure 2B). Plasma eNAMPT levels in 18-month-old ANKI mice were comparable to those in 6-month-old control mice (Figure S2A). Adipose tissue *Nampt* overexpression was maintained ~1.5-fold higher in aged ANKI mice, compared to that in control mice, confirming that *Nampt* overexpression was in the physiological range and suggesting that the ANKI model is physiologically valid (data not shown).

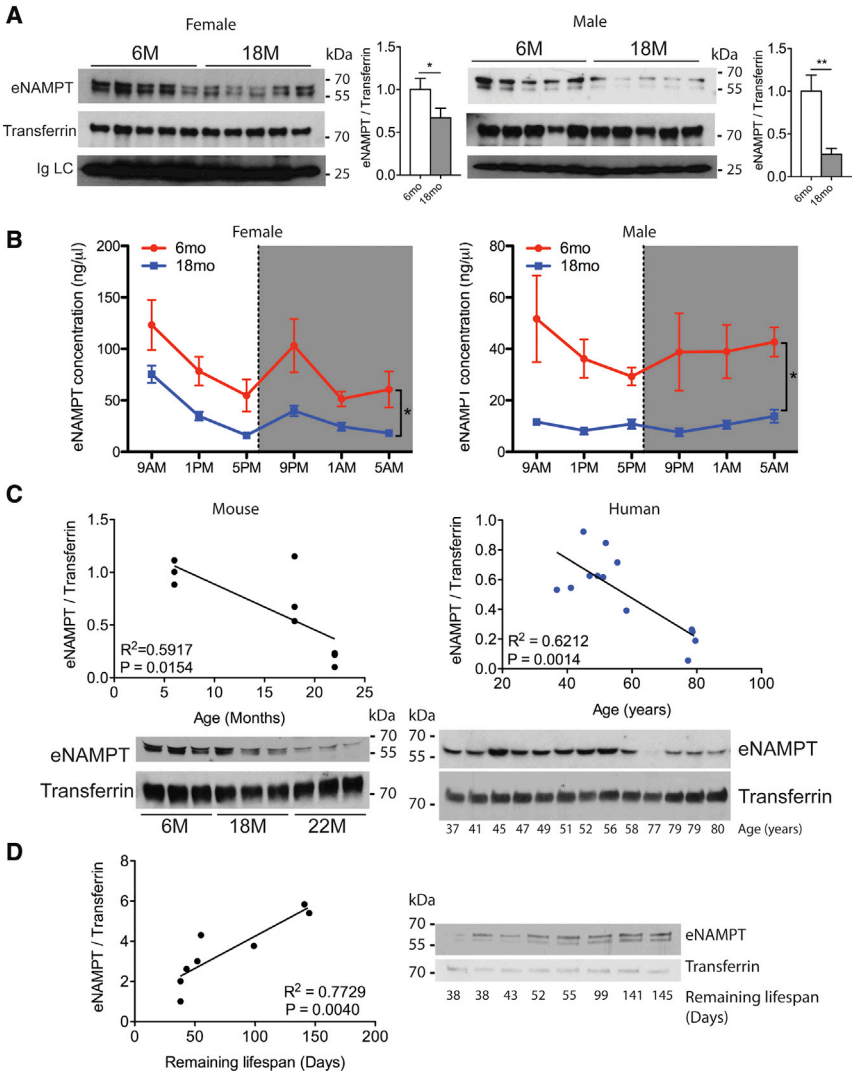


**Figure 1. Plasma eNAMPT Levels Are Reduced with Age in Both Mice and Humans and Predicts Remaining Lifespans of Individual Mice**

(A) Plasma eNAMPT levels of female and male mice at 6 and 18 months of age (n = 5).

(B) Plasma eNAMPT concentrations of female and male mice at 6 and 18 months of age over a 24-hr period (n = 5 per time point per age). The differences between plasma eNAMPT levels at 6 and 18 months of age were assessed by two-way repeated measures ANOVA and the age effects were significant in both males and females ($p < 0.05$).

(C) Plasma eNAMPT levels of mice and humans across different age groups (n = 9 for mice; n = 13 for humans).

(D) Relationship of plasma eNAMPT levels and the remaining lifespans of individual mice (n = 8). eNAMPT levels were measured at 26–28 months of age.

In *ad libitum*-fed 20-month-old ANKI mice, increased $NAD^+$ levels were observed in the hypothalamus, hippocampus, pancreas, and retina in females, whereas only pancreas and retina showed increased $NAD^+$ levels in males (Figures 2C and S2B). It should be noted that those tissues that showed increased $NAD^+$ levels in aged ANKI mice are the ones that have relatively very low levels of iNAMPT (Revollo et al., 2007; Stein et al., 2014; Yoon et al., 2015). These results suggest that adipose-tissue-specific overexpression of *Nampt* mitigates age-dependent decline in circulating eNAMPT levels and tissue $NAD^+$ levels in multiple tissues including the hypothalamus, hippocampus, pancreas, and retina.

## Aged ANKI Mice Display Significant Enhancement in Physical Activity and Sleep Quality

Given that hypothalamic $NAD^+$ levels increased in aged ANKI female mice and also that hypothalamic SIRT1 activity is critical to regulate physical activity and sleep quality during aging (Satoh et al., 2013; Satoh et al., 2015), we examined these age-associated physiological traits in aged ANKI mice. Consistent with the reduction in circulating eNAMPT levels with age, wheel-running activity during the dark time was significantly reduced in 18-month-old wild-type mice, compared to that in 6-month-old wild-type mice (Figure S3A). ANKI female mice at 4 months of age exhibited equivalent levels of wheel-running activity during the dark time to those of age-matched control mice, whereas ANKI female mice at 18 months of age showed significantly enhanced wheel-running activity compared to that in the age-matched control mice, similar to the activity levels in 6-month-old wild-type mice (Figures 3A and S3A). Additionally, we evaluated locomotor activity in the open field in these mice. Consistent with wheel-running activity during the dark time, aged ANKI female mice showed significantly higher total ambulatory and rearing activities, compared to the age-matched control mice (Figure 3B). However, aged ANKI male mice failed to show any significant differences in total ambulatory and rearing activities, compared to the age-matched control mice (Figure S3B), consistent with the lack of $NAD^+$ increase in the hypothalamus (Figure 2C).

In humans, it has been well documented that the number of sleep-wake transitions increases over age, a phenomenon called sleep fragmentation (Mander et al., 2017). Consistent with such changes in the older humans, 20-month-old wild-type mice also showed increased numbers of transitions between non-REM (NREM) sleep and wake cycles, compared to those in 4-month-old wild-type mice (Figure 3C, left), indicating that sleep fragmentation significantly increases with age in mice. There were no differences in the numbers of transitions between REM sleep and wake or NREM sleep cycles (data not shown). Interestingly, compared to the age-matched control mice, aged ANKI mice showed a significant reduction in the numbers of transitions between NREM sleep and wake cycles, which maintained levels similar to those seen in 4-month-old

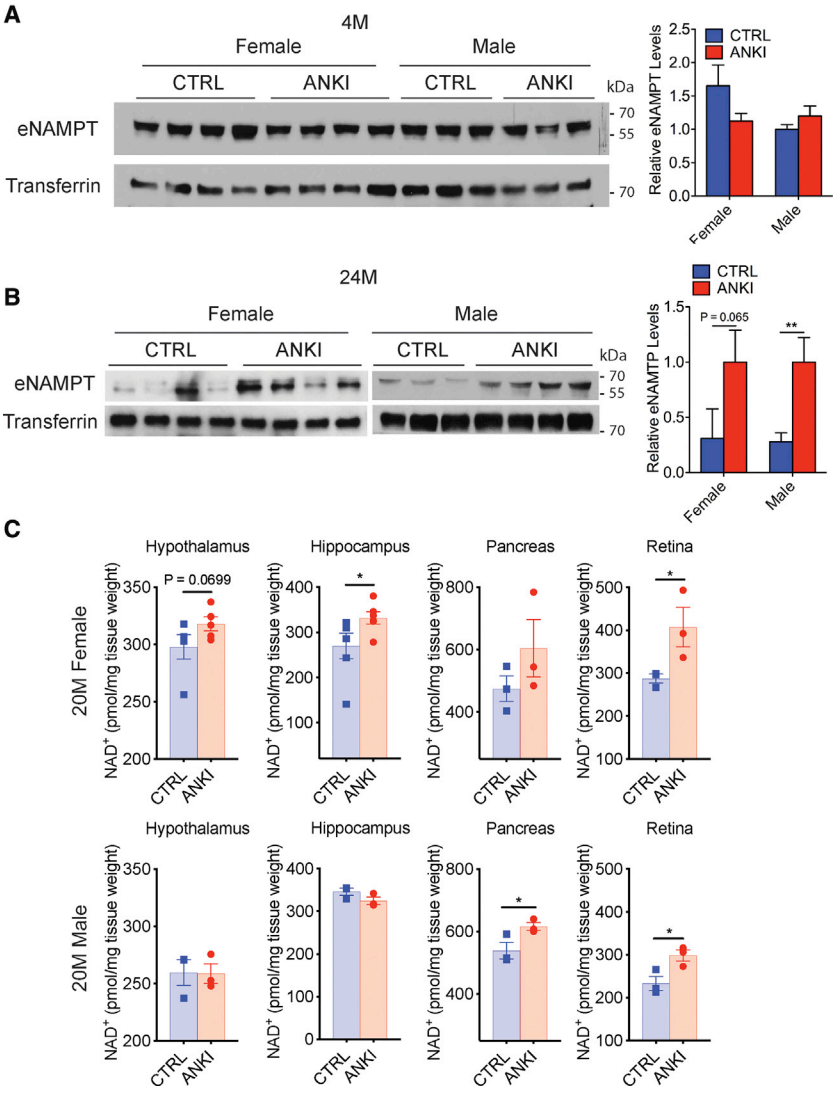


**Figure 2. Adipose-Tissue-Specific Overexpression of *Nampt* Maintains Higher Plasma eNAMPT Levels and NAD⁺ Biosynthesis in Multiple Tissues during Aging**

(A) Plasma eNAMPT levels of control (CTRL) and ANKI mice at 4 months of age (n = 3–4 per group per sex).

(B) Plasma eNAMPT levels of control and ANKI mice at 24 months of age (n = 3–4 per group per sex).

(C) Tissue NAD⁺ levels of control and ANKI mice at 20 months of age (n = 3 per group per sex).

## Aged ANKI Mice Show Significant Improvement in Glucose-Stimulated Insulin Secretion, Photoreceptor Function, and Cognitive Function

Because pancreatic, retinal, and hippocampal NAD⁺ levels were increased in aged ANKI mice (Figure 2C), we suspected that they might also exhibit improvements in glucose metabolism, retinal function, and cognitive function. We first performed intraperitoneal glucose tolerance tests (IPGTTs) in aged ANKI and control mice. We observed a moderate but significant improvement in glucose tolerance in aged ANKI male mice (Figure 4A). During IPGTTs, we also detected a significant increase in glucose-stimulated insulin secretion at the 30-min time point (Figure 4B). The results from insulin tolerance tests did not differ between aged ANKI and control mice, both showing severe insulin resistance (Figure S4A), suggesting that improved glucose tolerance in aged ANKI mice is mainly because of increased insulin secretion. Interestingly, aged ANKI mice possessed a higher total number of islets, compared to age-matched controls (Figures 4C and 4D). Additionally, those islets observed in aged ANKI males were kept smaller than those in age-matched controls (Figure 4E). These results are consistent with the role of NAD⁺ biosynthesis and SIRT1 in promoting glucose-stimulated insulin secretion in pancreatic β cells and protecting them from stresses (Kitamura et al., 2005; Moynihan et al., 2005; Ramsey et al., 2008; Revollo et al., 2007). Aged ANKI female mice also maintained a higher total number of islets but did not show any improvement in glucose tolerance (data not shown), consistent with a much larger variability in pancreatic NAD⁺ levels (Figure 2C). Aged ANKI female mice showed moderate increases in body weight and fat mass, whereas aged ANKI male mice showed no difference (Figures S4B and S4C). Furthermore, their food intake did not show any significant differences, compared to their age-matched controls (Figure S4D). We also examined circulating levels of proinflammatory cytokines in aged ANKI mice. There were no significant changes in circulating proinflammatory cytokine levels in both aged ANKI males and females, except for slight increases in IL-2 and moderate decreases in G-CSF in aged ANKI females (Figure S4E). Thus, wild-type mice (Figure 3C, right), implying that aged ANKI mice maintain a better quality of sleep.

These age-associated activity and sleep traits are regulated by hypothalamic SIRT1 through the regulation of its downstream target genes, *Orexin type-2 receptor* (*Ox2r*) and *PR domain 13* (*Prdm13*) (Satoh et al., 2013, 2015). *Ox2r* expression is important for the control of wheel-running activity during the dark time (Satoh et al., 2013), whereas *Prdm13* expression is critical for the maintenance of sleep quality (Satoh et al., 2015). Thus, we examined mRNA expression levels of *Ox2r* and *Prdm13* in the hypothalami of age-matched control and ANKI female mice. Consistent with the observed enhancement of physical activity and sleep quality, hypothalamic *Ox2r* and *Prdm13* expression levels were significantly increased in aged ANKI female mice, compared to those in age-matched control mice (Figure 3D). These results indicate that an age-associated decline in circulating eNAMPT levels contributes to the reduction in hypothalamic NAD⁺ levels and SIRT1 activity, resulting in the age-associated decline in physical activity and sleep quality, and that these functional reductions can be ameliorated by increasing circulating eNAMPT.

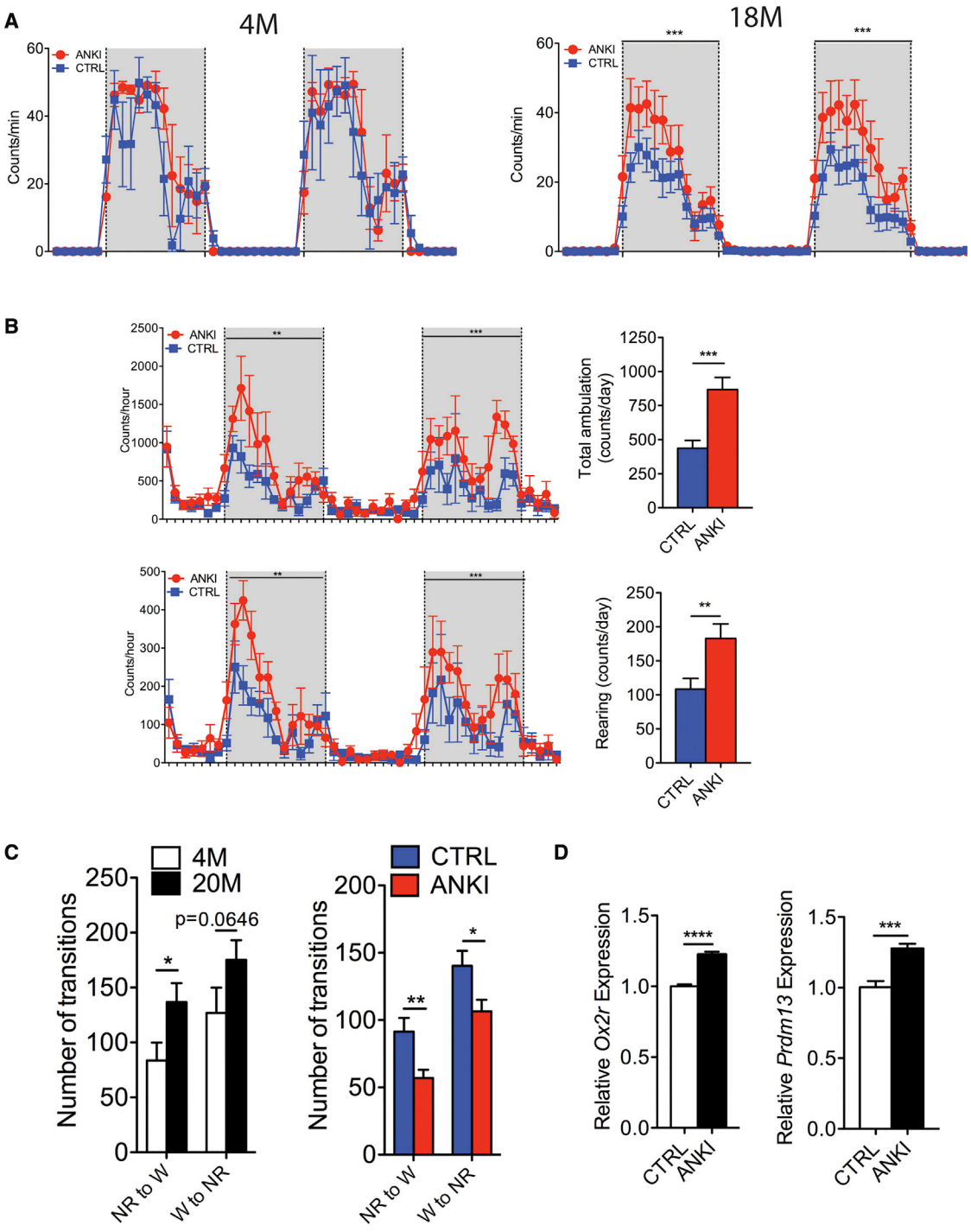


**Figure 3. Aged ANKI Mice Display Significant Enhancement of Physical Activity and Sleep Quality**

(A) Wheel-running activity of control (CTRL) and ANKI female mice at 4 and 18 months of age (4-month-old, n = 3; 18-month-old, n = 10–13 per group).

(B) Total ambulatory (upper panel) and rearing (lower panel) activities of control and ANKI female mice at 18 months of age (n = 4–5 per group).

(C) The levels of sleep fragmentation in 4- and 20-month-old male mice (n = 6 per group) and control and ANKI mice at 20 months of age (n = 7–8 per group; male and female mice combined). The numbers of transitions between NREM sleep (NR) and wake (W) cycles are shown.

(D) mRNA expression levels of *Ox2r* and *Prdm13* in the hypothalami of control and ANKI female mice at 20 months of age (n = 3–6 per group).

the observed ANKI phenotypes in glucose metabolism are unrelated to body weight, adiposity, or proinflammatory cytokine levels.

We next conducted electroretinography to examine retinal function under rod- and cone-dominated testing conditions. We found that, compared to age-matched control mice, aged

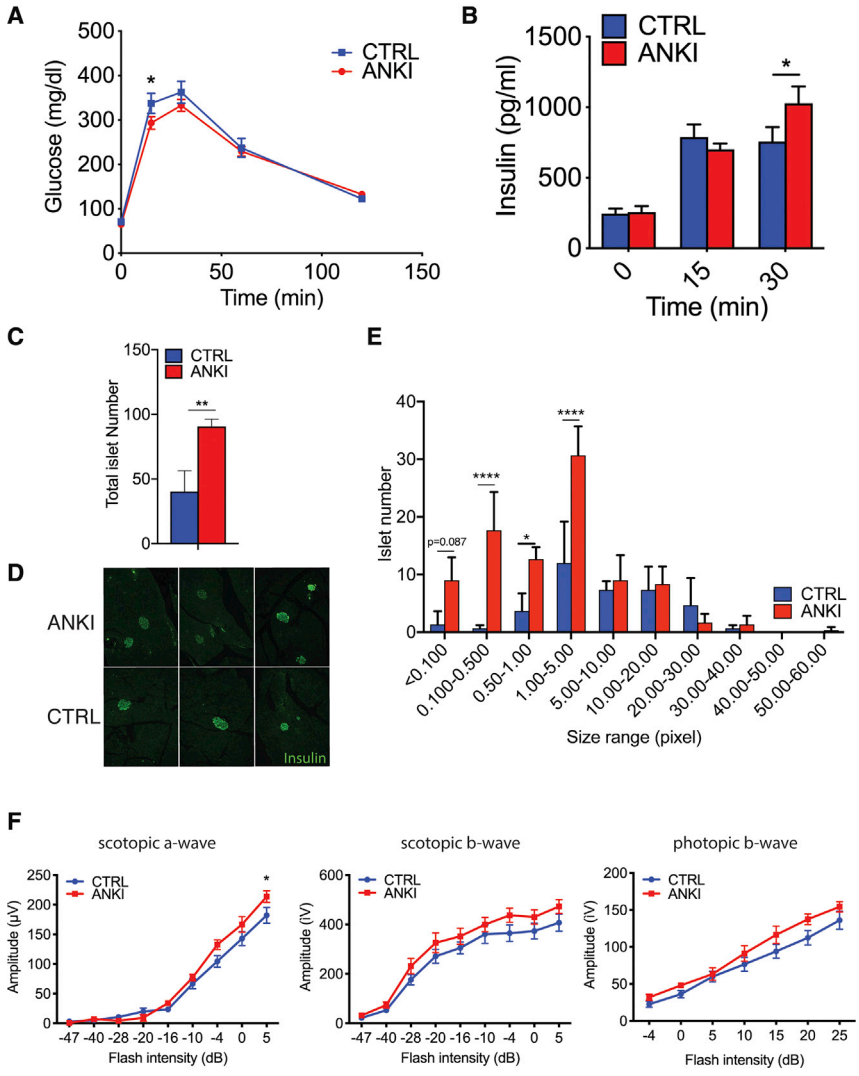


**Figure 4. Aged ANKI Mice Show Significant Improvement in Glucose Tolerance, Insulin Secretion, and Photoreceptor Function**

(A and B) Blood glucose (n = 8–13) (A) and insulin (n = 8–9) (B) levels during the IPGTTs in control (CTRL) and ANKI male mice at 17–20 months of age.

(C–E) Total numbers (C), representative images (D), and size distributions (E) of pancreatic islets in the pancreata of control and ANKI male mice at 20 months of age (n = 3 per group).

(F) Scotopic a, scotopic b, and photopic b-waves from ERG analysis of control and ANKI mice at 18–20 months of age (n = 6–7 per group; male and female combined).

ANKI mice showed significantly higher scotopic a-wave amplitudes at 5 db and a trend toward higher scotopic a-wave amplitudes at −4 and 0 db. (Figure 4F, left), indicating improved rod photoreceptor function. Similarly, improvement in rod photoreceptor function also led to trends toward enhanced scotopic b-waves (Figure 4F, middle). We also observed trends toward enhanced photopic b-wave amplitudes in aged ANKI mice, which suggest enhanced cone function (Figure 4F, right). Of interest, these changes are remarkably similar to those observed in the long-term NMN administration (Mills et al., 2016).

We also performed contextual fear conditioning tests on aged ANKI and age-matched control mice to assess their nonspatial hippocampus-dependent learning and memory capabilities. Both mice showed equivalent responses during the baseline and training trials on day 1 (Figure S4F, left). However, during the first minute of the contextual fear conditioning test on day 2, aged ANKI mice exhibited significantly higher levels of freezing, compared to age-matched controls (Figure S4F, middle). A similar trend was also observed at 2 and 3 min time points during this trial. Throughout the baseline and the auditory cue tests on day 3, aged ANKI and age-matched control mice did not show any significant differences (Figure S4F, right). Consistent with their hippocampal $NAD^+$ increases, these results suggest that aged ANKI mice maintain a better hippocampus-dependent cognitive function, compared to their age-matched controls. Thus, taken together, these findings provide further support to the physiological significance of eNAMPT in the maintenance of tissue functions, such as the hypothalamus, hippocampus, pancreas, and retina, during aging by enhancing systemic $NAD^+$ biosynthesis.

## ANKI Female Mice Exhibit Significant Extension of Median Lifespan and Delay in Aging

Because maintaining higher eNAMPT levels significantly mitigates age-associated functional decline in aged ANKI mice, we set up cohorts of ANKI and control mice to examine their lifespan. When fed regular chow *ad libitum*, ANKI female mice showed statistically significant extension (13.4%) of median lifespan (control 693 days versus ANKI 786 days, Gehan-Breslow-Wilcoxon test, $\chi^2 = 6.043$, df = 1, p = 0.014) (Figures 5A and 5B). Their maximal lifespan did not differ from that of control mice (Figure 5B). Interestingly, ANKI female mice exhibited significant delays in age-associated mortality up to ~2 years of age (Figure 5C). However, toward the end of their lifespan, the difference in age-associated mortality was no longer present, which could explain the lack of maximal lifespan extension. Although neoplasms are a major cause of death, the incidence and the type of neoplasms did not differ between ANKI and control mice (Figure 5D). In contrast to females, ANKI male mice exhibited no lifespan extension (Figures 5A and 5B) and no difference in age-associated mortality rate throughout the majority of their lifespan (Figure 5C), although the oldest 10% ANKI males showed a significantly longer maximal lifespan compared to control mice. These results demonstrate that maintaining youthful levels of circulating eNAMPT is critical to delay aging and extend healthspan in mice, although there is a significant sex difference.

A

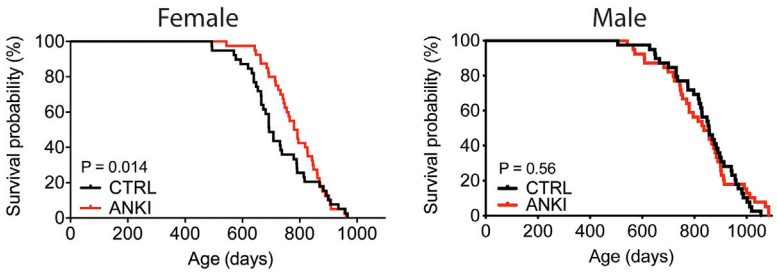


B

| | | n | Mean (days) | Median (days) | P value by Wilcoxon test | Min-Max (in 20% oldest) | Oldest 10% | Oldest 20% |
|---|---|---|---|---|---|---|---|---|
| Female | Control | 39 | 728 ± 20 | 693 | 0.014 | 869-967 | 942 ± 13 | 914 ± 13 |
| | ANKI | 40 | 786 ± 15 ** | 786 | | 871-962 | 933 ± 15 | 909 ± 12 |
| Male | Control | 39 | 844 ± 20 | 856 | 0.56 | 959-1055 | 1022 ± 12 | 998 ± 11 |
| | ANKI | 39 | 826 ± 23 | 836 | | 914-1085 | 1068 ± 13 * | 1024 ± 21 |

C

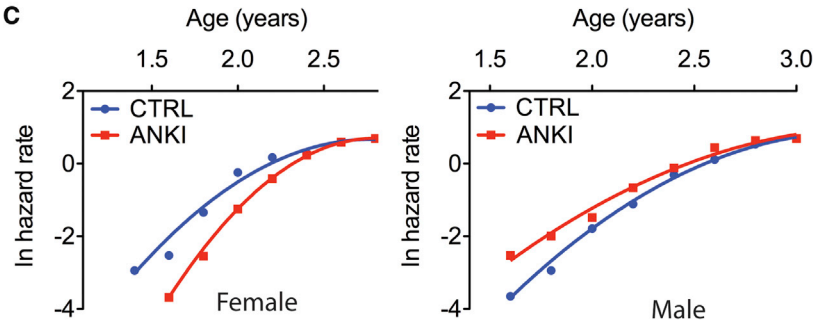


D

| | CTRL | % | ANKI | % |
|---|---|---|---|---|
| Neoplasm | 29 | 67.4 | 26 | 60.5 |
| Sarcoma | 22 | 51.2 | 18 | 41.9 |
| Lymphoma | 3 | 7.0 | 4 | 9.3 |
| Carcinoma | 3 | 7.0 | 2 | 4.7 |
| Leukemia | 1 | 2.3 | 2 | 4.7 |
| Other | 6 | 14.0 | 6 | 14.0 |
| Non-neoplasm* | 8 | 18.6 | 11 | 25.6 |

*Septicemia, urinary tract obstruction, thromboembolism, cardiomyopathy, fecal impaction

**Figure 5. Female ANKI Mice Exhibit Significant Extension of Median Lifespan and Delay in Aging**

(A) Kaplan-Meier curves of female and male ANKI mice (females, control 39, ANKI 40; males, control 39, ANKI 39).

(B) Lifespan parameters of control and ANKI mice. Mean and maximal lifespans of the oldest 10% and 20% of each cohort are shown as mean values ± SEM. The differences in survival curves and mean lifespans were assessed by Gehan-Breslow-Wilcoxon test and Student's t test, respectively.

(C) Age-associated mortality rates of control and ANKI female and male mice.

(D) Identified causes of death in aged control and ANKI mice (n = 37). Sarcoma subtypes include histio-, hemangio-, lipo-, and fibrosarcoma, while carcinoma subtypes include hepatocellular, bronchiolo-alveolar, and cholangiocarcinoma.

## Plasma eNAMPT Is Localized Exclusively to EVs

How circulating eNAMPT enhances tissue $NAD^+$ biosynthesis has so far remained elusive. Our finding that eNAMPT enhances $NAD^+$ biosynthesis in a tissue-specific manner suggested a possibility that circulating eNAMPT could directly contribute to $NAD^+$ biosynthesis in its target tissues. In recent years, a transport mechanism of microRNA by EVs from one tissue to another has drawn much attention as an important mechanism of intertissue communications (Whitham et al., 2018; Ying et al., 2017; Zhang et al., 2017). Thus, we asked whether eNAMPT could also be transported by EVs in systemic circulation. We purified EVs from mouse plasma by conventional ultracentrifugation or by using a polymer-based total exosome isolation (TEI) kit. Whereas the yield of EVs from the TEI method was much higher than ultracentrifugation, both methods clearly showed that eNAMPT was highly enriched in the EV fraction, compared to whole plasma or the remaining non-EV fraction (Figure 6A). The localization of eNAMPT in EVs was also confirmed by the enrichment of several EV markers including TG101, CD63, CD81, and CD9, and the depletion of transferrin and albumin. We also further purified the EV fractions from the TEI or ultracentrifugation by their floatation into a sucrose-density gradient. In both EV fractions, eNAMPT was clearly detected with several other EV markers, including Alix, TSG101, CD63, CD81, and CD9, in the third fraction from the sucrose-density gradient (Figures 6B and S5A). Additionally, we measured the densities of the fractions carrying eNAMPT-containing EVs isolated by the TEI method. eNAMPT was copurified with one of EV markers, Alix, in previously reported density fractions for EVs that range between 1.10 and 1.15 (Figure S5B) (Ying et al., 2017). We also examined whether eNAMPT in human plasma was contained in EVs. Consistent with mouse eNAMPT, human plasma eNAMPT was mainly contained in the EV fraction (Figure 6C). The proper enrichment of EVs from mouse and human plasma was further confirmed by electron microscopy (Figures S5C and S5D), which shows that the type of EVs purified from mouse and human plasma is consistent with the one characterized as small EVs (Durcin et al., 2017). Unfortunately, our attempt at immunogold labeling for EV-contained eNAMPT failed because of the unavailability of an appropriate antibody for this purpose. Thus, we examined whether eNAMPT in the plasma is protected from the protease treatment because of its localization within the EVs. Whereas the treatment of plasma with proteinase K nearly completely digested circulating plasma proteins such as transferrin and immunoglobulin light chain, eNAMPT and an EV marker TSG101 exhibited resistance to proteinase K digestion (Figure 6D). Furthermore, upon adding a detergent (Triton-X) to dissolve the lipid bilayer of the EVs, the proteinase K treatment was able to eliminate eNAMPT and TSG101. These findings further confirmed that eNAMPT secreted into blood circulation was encapsulated into the EVs. By using cultured OP9 adipocytes, we also confirmed that fully differentiated adipocytes secrete EVs that contain eNAMPT and other EV marker proteins,

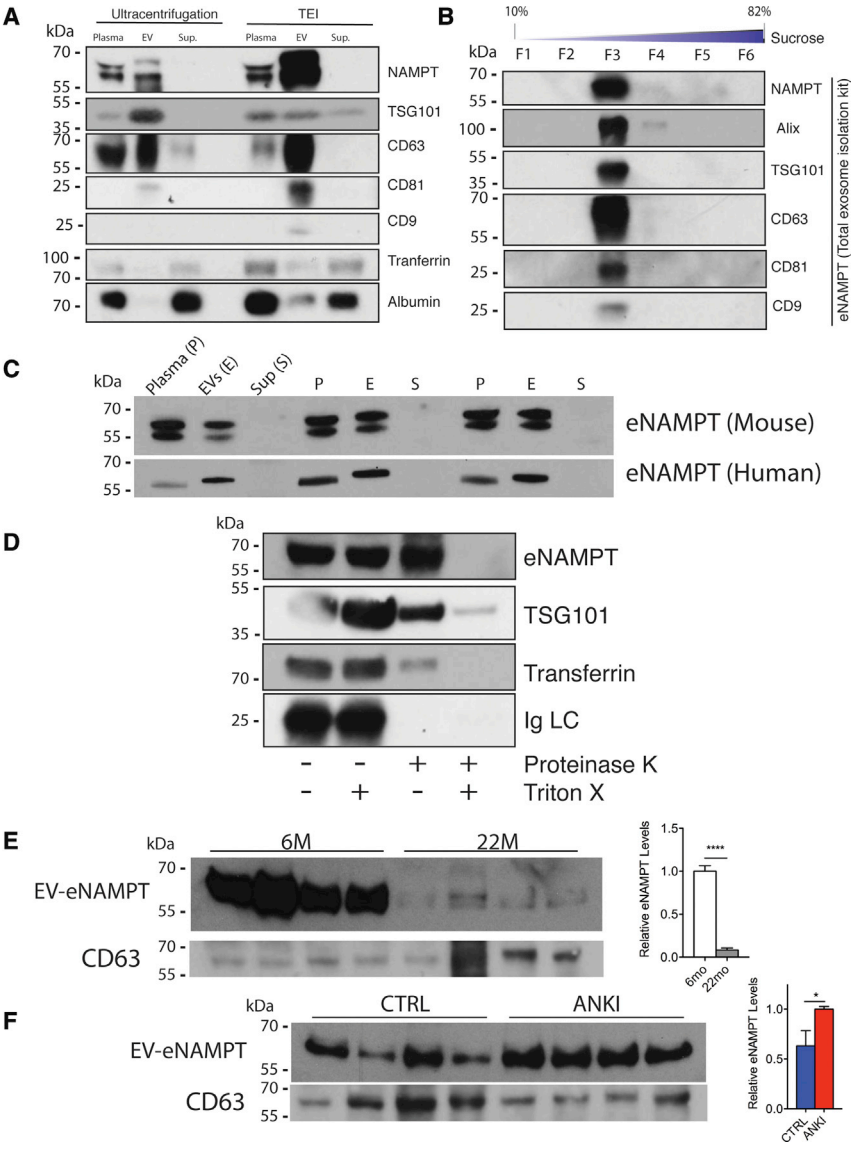


**Figure 6. Plasma eNAMPT Is Exclusively Localized to EVs in Both Mice and Humans**

(A) Comparison of eNAMPT, EV marker proteins (TSG101, CD63, CD81, and CD9), and non-EV proteins (transferrin and albumin) in whole plasma, EV fraction, and supernatant isolated by ultracentrifugation and the total exosome isolation (TEI) kit. The protein concentrations were typically ~0.4 and ~1 μg/μL for EVs purified by ultracentrifugation and the TEI kit, respectively, when EVs were reconstituted with an equal volume of PBS to the starting volume of plasma. 40 μg of protein from each fraction were loaded.

(B) Comparison of eNAMPT and EV marker proteins in six fractions (F1–F6) isolated from sucrose density-gradient centrifugation. 2 mL of plasma were used for this fractionation.

(C) Comparison of eNAMPT in whole plasma (P), EV fraction (E), and supernatant (S) isolated from three 4-month-old male mice and 37-, 41-, and 45-year-old male human donors. Each fraction was loaded after adjusting them to an equal volume.

(D) Comparison of eNAMPT, TSG101, transferrin, and immunoglobulin light chain (Ig LC) in the treatment of mouse plasma with proteinase K and/or Triton-X-100.

(E) Levels of EV-contained eNAMPT (EV-eNAMPT) and CD63 in the plasma from 6- and 22-month-old mice (n = 4 per group).

(F) Levels of EV-contained eNAMPT (EV-eNAMPT) and CD63 in the plasma of control (CTRL) and ANKI mice at 24 month of age (n = 4 per group).

but not other secreted proteins such as adiponectin and adipsin (Figure S5E).

We found that the eNAMPT content in EVs dramatically decreased from 6 to 22 month-old mice (Figure 6E). We also found that the content of eNAMPT in EVs from 24-month-old ANKI mice was significantly higher than that in age-matched control mice (Figure 6F). These observed changes in EV-contained eNAMPT levels were physiologically important because proteomic comparisons of EV-contained proteins between young (6-month-old) and aged (24-month-old) mice and between aged ANKI and control mice demonstrated that only a small fraction (2%–3%) of EV-contained proteins (181 proteins identified) exhibited significant changes in these conditions, and none of these proteins are related to $NAD^+$ metabolism (Figure S5F). Taken together, our results demonstrate that eNAMPT in mouse and human circulation is carried by EVs and also that changes in plasma eNAMPT levels observed during aging or in ANKI mice are due to the changes specific to EV-contained eNAMPT.

## EV-Contained eNAMPT Is Internalized into Cells and Directly Enhances $NAD^+$ Biosynthesis

Having demonstrated eNAMPT localization within EVs, we next examined whether EV-contained eNAMPT could be internalized into cells and enhance $NAD^+$ biosynthesis intracellularly. We first labeled isolated EVs with the BODIPY TR Ceramide, a red-fluorescent dye that can label lipid bilayers of EVs, and then incubated primary hypothalamic neurons with these BODIPY-labeled EVs. Primary hypothalamic neurons were labeled only when adding BODIPY-labeled EVs, but not when adding control BODIPY-treated media, suggesting that EVs were incorporated into primary hypothalamic neurons (Figure 7A). Next, we added bacterially produced FLAG-tagged recombinant NAMPT alone or FLAG-tagged recombinant NAMPT encapsulated into EVs to primary hypothalamic neurons. Interestingly, only EV-contained FLAG-tagged NAMPT was internalized into the cytoplasmic fraction of primary hypothalamic neurons (Figure 7B). When incorporating FLAG-tagged recombinant NAMPT into purified EVs, these EVs with an additional amount of NAMPT were able to increase intracellular $NAD^+$ levels in primary hypothalamic neurons (Figure 7B, right panel). To further confirm the effects of EV-contained eNAMPT on cellular $NAD^+$ biosynthesis, we measured the $NAD^+$ biosynthetic rate using isotopically labeled nicotinamide (D-4-NAM) in primary hypothalamic neurons. Both EVs (1 μg/μL as protein

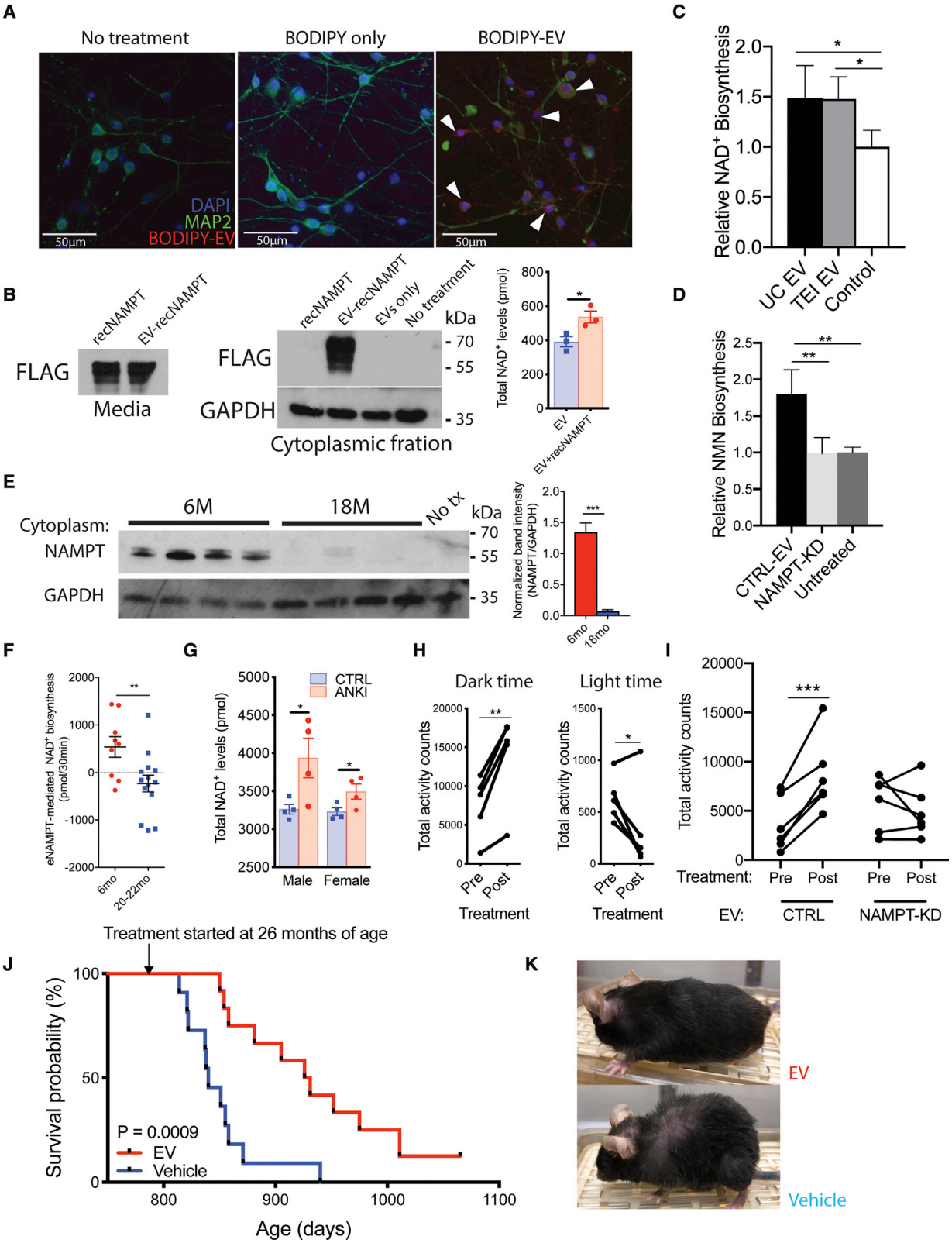


*(legend on next page)*

concentration) purified from mouse plasma by ultracentrifugation and the TEI method showed equivalent increases in $NAD^+$ biosynthesis compared to controls (Figure 7C). To examine whether the observed effects on $NAD^+$ biosynthesis are due to the enzymatic activity of EV-contained eNAMPT, we used EVs purified from the culture media of OP9 adipocytes by ultracentrifugation. We confirmed that ultracentrifugation-purified EVs from OP9 adipocytes were internalized properly to primary hypothalamic neurons (Figure S6A). Using this OP9 adipocyte system, we demonstrated that concentrated EVs from OP9 culture media, but not the EV-depleted supernatant, showed significant enhancement of NMN biosynthesis in primary hypothalamic neurons (Figure S6B). Then we compared the effects of EVs purified from the media of control and *Nampt*-knockdown (*Nampt*-KD) OP9 adipocytes on the NMN biosynthesis in primary hypothalamic neurons. The NAMPT expression was reduced by 80% in EVs secreted from *Nampt*-KD OP9 adipocytes (Figure S6C). Whereas EVs purified from the culture media of control OP9 adipocytes clearly showed the enhancement of NMN biosynthesis, EVs purified from the culture media of *Nampt*-KD OP9 adipocytes showed no enhancement of NMN biosynthesis in primary hypothalamic neurons (Figure 7D), demonstrating that these effects of EVs to stimulate cellular NMN/$NAD^+$ biosynthesis is primarily due to EV-contained eNAMPT.

The internalization of EV-contained eNAMPT into the cytoplasm of primary hypothalamic neurons was also examined by using mouse plasma and purified EVs from 6- and 18-month-old mice (Figures S6D and 7E). The amounts of internalized NAMPT in the cytoplasm mirrored the amounts of eNAMPT contained in original plasma or purified EVs, indicating that EVs from young mice can deliver higher amounts of eNAMPT into cells, compared to those from aged mice. We next compared the capabilities of EVs purified from young and aged mouse plasma to stimulate $NAD^+$ biosynthesis in primary hypothalamic neurons. Increments in intracellular $NAD^+$ levels were significantly higher with EVs from 6-month-old mice compared to those from 20 to 22-month-old mice (Figure 7F). Furthermore, EVs from ANKI male and female mice were able to increase intracellular $NAD^+$ levels in primary hypothalamic neurons, compared to those from age-matched control mice (Figure 7G). These results provide compelling evidence that EV-contained eNAMPT, which is internalized into target cells, can contribute to the enhancement of NMN/$NAD^+$ biosynthesis within its target cells.

## Supplementation with EV-Contained eNAMPT Enhances Wheel-Running Activity and Extends Lifespan in Aged Mice

Given that EV-contained eNAMPT was able to enhance intracellular $NAD^+$ levels in primary hypothalamic neurons, we reasoned that supplementation with eNAMPT-containing EVs could convey similar anti-aging effects on aged wild-type mice, as observed in aged ANKI mice. To test this possibility, we injected EVs purified from the plasma of 4–6-month-old mice intraperitoneally into 20-month-old wild-type female mice for four consecutive days. Remarkably, supplementation with EVs purified from young mouse plasma significantly enhanced wheel-running activity in aged mice during the dark time, compared to PBS-injected age-matched control mice (Figures S6E and 7H). Interestingly, whereas the wheel-running activity during the dark time clearly increased, the activity during the light time decreased significantly, implying that those EV-injected aged mice may sleep better. To further confirm whether this effect is due to EV-contained eNAMPT, we compared wheel-running activities of aged wild-type female mice by injecting EVs purified from the culture media of control and *Nampt*-KD OP9 adipocytes. Whereas EVs purified from control OP9 culture media again exhibited significant increases and decreases in wheel-running activity during the dark and the light times, respectively, EVs purified from *Nampt*-KD OP9 culture media failed to show these effects (Figures 7I and S6F), demonstrating that this effect is mediated by EV-contained eNAMPT. A mild enhancement of wheel-running activity was also observed in aged male mice (Figure S6G), suggesting that male mice can also respond to high levels of EV-contained eNAMPT supplementation.

We then tested whether eNAMPT-containing EVs purified from young mouse plasma could extend the lifespan of aged mice. We started injecting EVs purified from young-to-middle age (4–12-month-old) mice once a week into female mice at 26 months of age. Remarkably, supplementation with EVs purified from young-to-middle-aged mice significantly extended the lifespan of aged mice (Figure 7J). The median lifespan was extended by 10.2% (840 days for vehicle-injected mice versus

**Figure 7. EV-Contained eNAMPT Directly Enhances $NAD^+$ Biosynthesis in Primary Hypothalamic Neurons and Ameliorates Age-Associated Decline in Physical Activity and Extends Lifespan in Mice**

(A) Fluorescent images of primary hypothalamic neurons following the incubation with BODIPY-labeled EVs. EVs purified from 400 μL of mouse plasma were added to 200 μL of culture media. Arrowheads indicate neurons that internalized BODIPY-labeled EVs.

(B) Cytoplasmic levels of FLAG-tagged recombinant NAMPT (recNAMPT) and cellular $NAD^+$ levels in the primary hypothalamic neurons after incubated with recNAMPT alone or EV-contained recNAMPT (n = 3).

(C) Relative rate of $NAD^+$ biosynthesis in primary hypothalamic neurons after incubating with EVs isolated from plasma with ultracentrifugation and TEI kit (n = 4).

(D) Relative cellular NAMPT activity in primary hypothalamic neurons after incubating with control (CTRL) and *Nampt*-knockdown (NAMPT-KD) EVs generated from OP9 adipocytes (n = 3–6).

(E) Levels of cytoplasmic NAMPT and $NAD^+$ in primary hypothalamic neurons after incubated with EVs isolated from 6- and 18-month-old mice (n = 4).

(F) $NAD^+$ level changes after incubating with EVs isolated from 6- and 20–22-month-old mice. (n = 9–13)

(G) $NAD^+$ levels in primary hypothalamic neurons after incubating with EVs isolated from control (CTRL) and ANKI mice at 20 months of age.

(H) Total wheel-running activity counts of 20-month-old female mice during dark and light times before and after 4 consecutive daily injections of EVs purified from 4- to 6-month-old mice (n = 5).

(I) Total wheel-running activity counts of 25-month-old female mice during the dark time before and after 4 consecutive daily injections of control (CTRL) and *Nampt*-knockdown (NAMPT-KD) EVs purified from OP9 adipocytes (n = 6).

(J and K) Kaplan-Meier curves (J) and representative images (K) of aged female mice injected with vehicle or EVs isolated from 4- to 12-month-old mice (n = 11–12). The mouse images were taken after 3 months of treatment.

926 days for EV-injected mice, Gehan-Breslow-Wilcoxon test, $\chi^2 = 11.10$, df = 1, p = 0.0009), and two mice were still alive at the time of final manuscript preparation. The mean maximal lifespans of 4 longest-lived mice in each group were 881 ± 63.6 and 1020 ± 62 days for vehicle- and EV-injected mice, respectively (Student's t test, p = 0.0012, 15.8% extension). The EV-injected aged mice generally maintained much healthier looking and higher activity compared to vehicle-injected age-matched control mice (Figure 7K; Video S1). Taken together, these findings demonstrate that supplementation with EV-contained eNAMPT is an effective anti-aging intervention to mitigate age-associated functional decline and extend lifespan in mice.

## DISCUSSION

Our present study has demonstrated that EV-mediated systemic delivery of eNAMPT mitigates age-associated functional decline in specific target tissues including the hypothalamus, hippocampus, pancreas, and retina, delays age-associated mortality rate, and extends healthspan and lifespan in mice. The surprising finding in this study is that EV-contained eNAMPT is internalized into target cells and enhances NMN/$NAD^+$ biosynthesis intracellularly, whereas the NAMPT protein alone cannot be internalized by itself. This provides a critical resolution for a long-standing debate on the physiological importance and function of eNAMPT in mammals. Whereas eNAMPT can function as a systemic $NAD^+$ biosynthetic enzyme and enhance $NAD^+$, SIRT1 activity, and neural activation in the hypothalamus (Revollo et al., 2007; Yoon et al., 2015), eNAMPT has also been reported to function as a proinflammatory cytokine (Dahl et al., 2012). Given that eNAMPT in circulation is almost exclusively contained in EVs under physiological conditions and also that only EV-contained eNAMPT is properly internalized into the cytoplasmic fraction of cells, we suggest that the physiological relevance and function of eNAMPT is to maintain NMN/$NAD^+$ biosynthesis systemically, particularly in the tissues that have relatively low levels of iNAMPT, such as the hypothalamus, hippocampus, pancreas, and retina. Although the precise mechanism by which eNAMPT-containing EVs are targeted specifically to those tissues needs to be elucidated, this EV-mediated systemic delivery of eNAMPT is a novel intertissue communication mechanism that maintains $NAD^+$ homeostasis throughout the body and modulates the process of aging and lifespan in mammals.

### Systemic Decline in NAMPT-Mediated $NAD^+$ Biosynthesis Limits Tissue Functions during Aging

In mammals, NAMPT is the rate-limiting enzyme in a major $NAD^+$ biosynthetic pathway starting from nicotinamide, a form of vitamin $B_3$. It has now been well established that systemic $NAD^+$ availability declines dramatically over age, and that age-associated reduction in iNAMPT levels contributes to limiting $NAD^+$ availability in many tissues (Yoshino et al., 2018). We now show that circulating eNAMPT levels also decline with age in mice and humans, limiting $NAD^+$ availability in specific tissues that rely on eNAMPT-mediated $NAD^+$ biosynthesis. Adipose-tissue-specific overexpression of *Nampt* maintains circulating eNAMPT levels, resulting in significant enhancement in physical activity, sleep quality, glucose-stimulated insulin secretion, retinal photoreceptor function, and cognitive function in aged mice. These remarkable anti-aging effects of eNAMPT also contribute to the extension of median lifespan in mice. In aged ANKI mice, we did not observe any significant adverse effects of eNAMPT, including inflammation and cancer risks, arguing against the proposed primary function of eNAMPT as a proinflammatory cytokine.

Because circulating eNAMPT levels decline with age, an individual's capacity to sustain high levels of circulating eNAMPT must be important to maintain functional homeostasis of tissues over time, which likely determines a healthspan of each individual. The results from our small prospective study provides compelling support for this notion, showing a significant correlation between circulating eNAMPT levels and the remaining lifespan. Given that eNAMPT secretion from adipose tissue is regulated in a $NAD^+$/SIRT1-dependent manner (Yoon et al., 2015), the reservoir and/or the turnover of adipose $NAD^+$ could be a critical determinant for circulating eNAMPT levels and thereby lifespan. Interestingly, it has been reported that the effect of lifespan extension by diet restriction correlates inversely with fat reduction measured at mid-life and later ages, suggesting that certain factors associated with fat are important for survival and lifespan extension under diet restriction (Liao et al., 2011). Based on our results, it would be of great interest to examine whether eNAMPT secreted from adipose tissue is a significant contributor to the delayed aging and lifespan-extending effects of diet restriction.

### Genetic Supplementation of eNAMPT Delays Aging and Extends Healthspan in Mice

Aged ANKI mice show remarkable enhancement of $NAD^+$ levels and tissue functions in the hypothalamus, hippocampus, pancreas, and retina. We have previously demonstrated that NAMPT-mediated $NAD^+$ biosynthesis and $NAD^+$-dependent sirtuins play important roles in regulating these tissue functions. In the hypothalamus, $NAD^+$/SIRT1 signaling is critical in controlling the process of aging and determining lifespan (Satoh et al., 2013). In the hippocampus, NAMPT plays an important role in the function of excitatory neurons (Stein et al., 2014), particularly neurons in the CA1 region (Johnson et al., 2018). In pancreatic β cells, NAMPT and SIRT1 are critical to regulate glucose-stimulated insulin secretion (Moynihan et al., 2005; Revollo et al., 2007). In the retina, NAMPT and mitochondrial sirtuins SIRT3/5 are essential for the function of rod and cone photoreceptor neurons (Lin et al., 2016; Mills et al., 2016). These tissues most likely represent a group of tissues that are the most vulnerable to $NAD^+$ decline. There may be other tissues to which eNAMPT is also targeted to maintain adequate $NAD^+$ biosynthesis. Considering that adipose tissue is a major source of circulating eNAMPT (Yoon et al., 2015), it will be important to further elucidate intertissue communications between adipose tissue and other tissues through EV-mediated eNAMPT delivery.

Interestingly, phenotypes of aged ANKI mice overlap with those of aged BRASTO mice (Satoh et al., 2013). Particularly, the enhancement of wheel-running activity and sleep quality are observed in both aged ANKI and BRASTO mice. Consistent with these phenotypes, the hypothalamic expression levels of *Ox2r* and *Prdm13*, two SIRT1 target genes responsible for those phenotypes (Satoh et al., 2013, 2015), are significantly increased in both mouse models. Nonetheless, whereas BRASTO mice

exhibit both median and maximal lifespan extension, ANKI mice show only median lifespan extension. This discrepancy between BRASTO and ANKI mice suggests an interesting possibility that the level of SIRT1 in hypothalamic neurons primarily determines a maximal level of their function and thereby limits maximal lifespan, whereas the level of circulating eNAMPT modulates the extent of hypothalamic neuronal function and thereby changes median lifespan accordingly. Given that continuous supplementation with eNAMPT-containing EVs extends median and maximal lifespan of aged mice, it is also possible that the effect of eNAMPT in ANKI mice might be hindered at a very late stage of aging by a reduction in adipose tissue mass.

One important remaining question is about sex-dependent differences in circulating eNAMPT levels and the effects of eNAMPT on tissue $NAD^+$ levels and functions. For example, whereas ANKI female mice show significant median lifespan extension compared to control mice, ANKI male mice show equivalent lifespan curves to control male mice. Such phenotypic preferences to females have also been observed in *Nampt*$^{+/-}$ heterozygous mice (Revollo et al., 2007), BRASTO mice (Satoh et al., 2013), and ANKO mice (Yoon et al., 2015). Therefore, female mice might have higher sensitivity to changes in eNAMPT and/or $NAD^+$ levels, and ANKI mice could provide a valuable model to address this question. Further investigation will be necessary to elucidate the molecular mechanisms of these sex-specific preferences.

### EV-Mediated Systemic Delivery of eNAMPT Is a Novel Intertissue Communication Mechanism that Controls Aging and Lifespan in Mice

In recent years, many studies have reported an important role of EVs as a new inter-cellular or intertissue communication tool for transporting proteins and microRNAs (Whitham et al., 2018; Ying et al., 2017; Zhang et al., 2017). Indeed, it has recently been demonstrated that adipose tissue is a major source of circulating EV-contained microRNAs that regulate gene expression in distant tissues (Thomou et al., 2017). In this context, it is intriguing that eNAMPT in blood circulation is contained almost exclusively in EVs. In adipose tissue, SIRT1-dependent deacetylation of lysine 53 on iNAMPT predisposes the protein to secretion (Yoon et al., 2015), implicating that this deacetylation might be involved in the process of incorporating the NAMPT protein into EVs. However, how eNAMPT-containing EVs are targeted specifically to certain tissues, such as the hypothalamus, hippocampus, pancreas, and retina, remains unknown. This EV-mediated delivery is critical for eNAMPT to be properly internalized into cells and enhance NMN/$NAD^+$ biosynthesis intracellularly. When giving the eNAMPT protein alone, the protein is not internalized properly. Thus, it will be of great importance to understand the mechanism by which eNAMPT-containing EVs are delivered and internalized to specific tissues.

Interestingly, eNAMPT-containing EVs are transferable from one individual to another. In particular, our finding that supplementing eNAMPT-containing EVs purified from young mice significantly enhances the wheel-running activity and extends lifespan in aged mice opens a new possibility that EV-contained eNAMPT could be used as an anti-aging biologic. Given that significant amounts of eNAMPT are contained in circulating EVs, it would be of great interest to further investigate the importance of EV-contained eNAMPT in other biological models, such as heterochronic parabiosis and plasma transfusion. In human blood, eNAMPT is also contained exclusively in EVs. Thus, it will be of great importance to evaluate a possible connection between EV-contained eNAMPT levels and the vulnerability to age-associated diseases and also whether EV-contained eNAMPT supplementation could convey anti-aging effects in humans.

## Conclusion

Our present study demonstrates the importance of a novel EV-mediated intertissue communication mechanism that delivers eNAMPT, a key $NAD^+$ biosynthetic enzyme, to specific tissues in controlling the process of aging and determining healthspan and lifespan in mice. Age-associated decline in the levels of circulating EV-contained eNAMPT limits $NAD^+$ availability and tissue functions in these target tissues, including the hypothalamus, hippocampus, pancreas, and retina. Supplementing EV-contained eNAMPT to aged mice genetically or pharmacologically mitigates age-associated physiological decline during aging and extends lifespan in mice. These findings open a new possibility to use the EV-mediated systemic delivery of eNAMPT as a biologic for an effective anti-aging intervention.

## Limitations of Study

In our study, it remains unclear whether the increase in physical activity has a causal contribution to healthspan and lifespan extension in aged ANKI and EV-injected mice. Nonetheless, because the increase in physical activity and healthspan/lifespan extension appear to be tightly associated in aged ANKI, BRASTO, NMN-treated, and EV-injected mice, it will be of great importance to examine the cause-effect relationship between these two events. Although we have so far not observed any increase in cancer incidence in any of the above mouse models, further careful investigation will be necessary to examine whether there is any relation between enhanced $NAD^+$ biosynthesis and cancer risk.

## STAR★METHODS

Detailed methods are provided in the online version of this paper and include the following:

- KEY RESOURCES TABLE
- CONTACT FOR REAGENT AND RESOURCE SHARING
- EXPERIMENTAL MODEL AND SUBJECT DETAILS
  - Animal Models
  - Human Subjects
  - Cell Culture
- METHOD DETAILS
  - Lifespan and Hazard Rate Analyses
  - Physical Activity
  - Sleep Analysis
  - Metabolic Assessments
  - Electroretinography
  - Small Cohort Prospective Lifespan Analysis
  - Western Blot Analysis of eNAMPT
  - Gene Expression Analysis
  - EV Purification and Characterization
  - Sucrose Gradient Fractionation Analysis of EVs

- Proteinase K Digestion Assay
- Proteomic Analysis of Plasma EVs
- Isolation of Primary Hypothalamic Neurons
- EV Internalization Assay
- Generation of Recombinant NAMPT-Containing EVs and Their Internalization Assay
- Wheel-Running Assay after EV Injection
- Lifespan Study of EV-Injected Mice

● QUANTIFICATION AND STATISTICAL ANALYSIS
- Data Analysis

## SUPPLEMENTAL INFORMATION

Supplemental Information can be found online at https://doi.org/10.1016/j.cmet.2019.05.015.

## ACKNOWLEDGMENTS

We thank Cindy Brace and Suellen Greco for their technical assistance. We also thank Erik Herzog for his support to wheel-running activity measurements, David Wozniak for locomotor activity analysis in the Animal Behavior Core, members of the Imai lab for critical comments and suggestions on this study, and staff members in the Core Facilities provided by the Diabetes Research Center (P30 DK020579) and Nutrition Obesity Research Center (P30 DK56341). This work was mainly supported by grants to S.I. from the National Institute on Aging (AG037457, AG047902), the American Federation for Aging Research, and the Tanaka Fund. A part of this study was also performed in a facility supported by the NCRR grant C06 RR015502. A.S. is supported by the JSPS KAKENHI (JP18H03186), AMED (JP18gm5010001h0001), the Takeda Science Foundation, and the Research Fund for Longevity Sciences from the National Center for Geriatrics and Gerontology (28–47). S.I. and A.S. are also collaborating in the Project for Elucidating and Controlling Mechanisms of Aging and Longevity, organized by the Japan Agency for Medical Research and Development (AMED). S.I. is also supported by the Uehara Memorial Foundation at the Institute of Biomedical Research and Innovation (IBRI). M.W. and his lab members are supported by U54 HD087011 (Intellectual and Developmental Disabilities Research Center). R.S.A and his lab members are supported by the NIH R01 EY019287, P30 EY02687 (Vision Core grant), U54 HD087011 (Intellectual and Developmental Disabilities Research Center), the Starr Foundation Carl Marshall Reeves and Mildred Almen Reeves Foundation, the Bill and Emily, Kuzma Family Gift for retinal research, a Physician-Scientist Award and a Nelson Trust Award from Research to Prevent Blindness, the Jeffrey Fort Innovation Fund, the Thome Foundation, and an unrestricted grant to the Department of Ophthalmology and Visual Sciences of Washington University School of Medicine from Research to Prevent Blindness. J.B.L. was supported by the Washington University in St. Louis Medical Scientist Training Program (NIH grant T32 GM007200), the Washington University Institute of Clinical and Translational Sciences (NIH grants UL1 TR002345, TL1 TR002344), and the VitreoRetinal Surgery Foundation.

## AUTHOR CONTRIBUTIONS

M.Y. and S.I. conceived this study and designed the experiments. M.Y. performed most of the experiments and S.I. supervised the entire study. A.S., N.R., and M.W. conducted sleep analyses. M.Y. and K.F.M. performed IPGTTs and ITTs. J.B.L. and R.S.A. conducted ERGs and analyzed photoreceptor functions. Y.S. conducted the mass spectrometric analysis of isotopically labeled metabolites. M.Y. and S.I. analyzed the entire data and wrote the manuscript.

## DECLARATION OF INTERESTS

S.I. receives a part of patent-licensing fees from MetroBiotech (USA) and Teijin Limited (Japan) through Washington University. R.S.A. is a co-founder of Metro Midwest Biotech. All other authors declare no financial interests.

Received: August 27, 2018
Revised: March 2, 2019
Accepted: May 17, 2019
Published: June 13, 2019

## REFERENCES

Cantó, C., Menzies, K.J., and Auwerx, J. (2015). NAD(+) metabolism and the control of energy homeostasis: A balancing act between mitochondria and the nucleus. Cell Metab. *22*, 31–53.

Dahl, T.B., Holm, S., Aukrust, P., and Halvorsen, B. (2012). Visfatin/NAMPT: A multifaceted molecule with diverse roles in physiology and pathophysiology. Annu. Rev. Nutr. *32*, 229–243.

Durcin, M., Fleury, A., Taillebois, E., Hilairet, G., Krupova, Z., Henry, C., Truchet, S., Trötzmüller, M., Köfeler, H., Mabilleau, G., et al. (2017). Characterisation of adipocyte-derived extracellular vesicle subtypes identifies distinct protein and lipid signatures for large and small extracellular vesicles. J. Extracell. Vesicles *6*, 1305677.

Fukuhara, A., Matsuda, M., Nishizawa, M., Segawa, K., Tanaka, M., Kishimoto, K., Matsuki, Y., Murakami, M., Ichisaka, T., Murakami, H., et al. (2007). Retraction. Science *318*, 565.

Garten, A., Schuster, S., Penke, M., Gorski, T., de Giorgis, T., and Kiess, W. (2015). Physiological and pathophysiological roles of NAMPT and NAD metabolism. Nat. Rev. Endocrinol. *11*, 535–546.

Imai, S. (2009). Nicotinamide phosphoribosyltransferase (Nampt): a link between NAD biology, metabolism, and diseases. Curr. Pharm. Des. *15*, 20–28.

Imai, S., and Guarente, L. (2014). $NAD^+$ and sirtuins in aging and disease. Trends Cell Biol. *24*, 464–471.

Imai, S.I. (2016). The NAD World 2.0: the importance of the inter-tissue communication mediated by NAMPT/NAD+/SIRT1 in mammalian aging and longevity control. NPJ Syst. Biol. Appl. *2*, 16018.

Johnson, S., Wozniak, D.F., and Imai, S. (2018). CA1 Nampt knockdown recapitulates hippocampal cognitive phenotypes in old mice which nicotinamide mononucleotide improves. NPJ Aging Mech. Dis. *4*, 10.

Kitamura, Y.I., Kitamura, T., Kruse, J.P., Raum, J.C., Stein, R., Gu, W., and Accili, D. (2005). FoxO1 protects against pancreatic beta cell failure through NeuroD and MafA induction. Cell Metab. *2*, 153–163.

Liao, C.Y., Rikke, B.A., Johnson, T.E., Gelfond, J.A., Diaz, V., and Nelson, J.F. (2011). Fat maintenance is a predictor of the murine lifespan response to dietary restriction. Aging Cell *10*, 629–639.

Lin, J.B., Kubota, S., Ban, N., Yoshida, M., Santeford, A., Sene, A., Nakamura, R., Zapata, N., Kubota, M., Tsubota, K., et al. (2016). NAMPT-mediated NAD(+) biosynthesis is essential for vision in mice. Cell Rep. *17*, 69–85.

Lin, J.B., Kubota, S., Mostoslavsky, R., and Apte, R.S. (2018). Role of sirtuins in retinal function under basal conditions. Adv. Exp. Med. Biol. *1074*, 561–567.

Mander, B.A., Winer, J.R., and Walker, M.P. (2017). Sleep and human aging. Neuron *94*, 19–36.

Mills, K.F., Yoshida, S., Stein, L.R., Grozio, A., Kubota, S., Sasaki, Y., Redpath, P., Migaud, M.E., Apte, R.S., Uchida, K., et al. (2016). Long-term administration of nicotinamide mononucleotide mitigates age-associated physiological decline in mice. Cell Metab. *24*, 795–806.

Moynihan, K.A., Grimm, A.A., Plueger, M.M., Bernal-Mizrachi, E., Ford, E., Cras-Méneur, C., Permutt, M.A., and Imai, S. (2005). Increased dosage of mammalian Sir2 in pancreatic beta cells enhances glucose-stimulated insulin secretion in mice. Cell Metab. *2*, 105–117.

Rajman, L., Chwalek, K., and Sinclair, D.A. (2018). Therapeutic potential of NAD-boosting molecules: the in vivo evidence. Cell Metab. *27*, 529–547.

Ramsey, K.M., Mills, K.F., Satoh, A., and Imai, S. (2008). Age-associated loss of Sirt1-mediated enhancement of glucose-stimulated insulin secretion in β cell-specific Sirt1-overexpressing (BESTO) mice. Aging Cell *7*, 78–88.

Revollo, J.R., Körner, A., Mills, K.F., Satoh, A., Wang, T., Garten, A., Dasgupta, B., Sasaki, Y., Wolberger, C., Townsend, R.R., et al. (2007). Nampt/PBEF/visfatin regulates insulin secretion in β cells as a systemic NAD biosynthetic enzyme. Cell Metab. *6*, 363–375.

Samal, B., Sun, Y., Stearns, G., Xie, C., Suggs, S., and McNiece, I. (1994). Cloning and characterization of the cDNA encoding a novel human pre-B-cell colony-enhancing factor. Mol. Cell. Biol. *14*, 1431–1437.

Satoh, A., Brace, C.S., Rensing, N., Cliften, P., Wozniak, D.F., Herzog, E.D., Yamada, K.A., and Imai, S. (2013). Sirt1 extends life span and delays aging in mice through the regulation of NK2 homeobox 1 in the DMH and LH. Cell Metab. *18*, 416–430.

Satoh, A., Brace, C.S., Rensing, N., and Imai, S. (2015). Deficiency of Prdm13, a dorsomedial hypothalamus-enriched gene, mimics age-associated changes in sleep quality and adiposity. Aging Cell *14*, 209–218.

Stein, L.R., Wozniak, D.F., Dearborn, J.T., Kubota, S., Apte, R.S., Izumi, Y., Zorumski, C.F., and Imai, S. (2014). Expression of Nampt in hippocampal and cortical excitatory neurons is critical for cognitive function. J. Neurosci. *34*, 5800–5815.

Thomou, T., Mori, M.A., Dreyfuss, J.M., Konishi, M., Sakaguchi, M., Wolfrum, C., Rao, T.N., Winnay, J.N., Garcia-Martin, R., Grinspoon, S.K., et al. (2017). Adipose-derived circulating miRNAs regulate gene expression in other tissues. Nature *542*, 450–455.

Verdin, E. (2015). $NAD^+$ in aging, metabolism, and neurodegeneration. Science *350*, 1208–1213.

Whitham, M., Parker, B.L., Friedrichsen, M., Hingst, J.R., Hjorth, M., Hughes, W.E., Egan, C.L., Cron, L., Watt, K.I., Kuchel, R.P., et al. (2018). Extracellular vesicles provide a means for tissue crosstalk during exercise. Cell Metab. *27*, 237–251.

Ying, W., Riopel, M., Bandyopadhyay, G., Dong, Y., Birmingham, A., Seo, J.B., Ofrecio, J.M., Wollam, J., Hernandez-Carretero, A., Fu, W., et al. (2017). Adipose tissue macrophage-derived exosomal miRNAs can modulate in vivo and in vitro insulin sensitivity. Cell *171*, 372–384.

Yoon, M.J., Yoshida, M., Johnson, S., Takikawa, A., Usui, I., Tobe, K., Nakagawa, T., Yoshino, J., and Imai, S. (2015). SIRT1-mediated eNAMPT secretion from adipose tissue regulates hypothalamic $NAD^+$ and function in mice. Cell Metab. *21*, 706–717.

Yoshino, J., Baur, J.A., and Imai, S.I. (2018). $NAD^+$ intermediates: the biology and therapeutic potential of NMN and NR. Cell Metab. *27*, 513–528.

Yoshino, J., Mills, K.F., Yoon, M.J., and Imai, S. (2011). Nicotinamide mononucleotide, a key NAD(+) intermediate, treats the pathophysiology of diet- and age-induced diabetes in mice. Cell Metab. *14*, 528–536.

Zhang, G., Li, J., Purkayastha, S., Tang, Y., Zhang, H., Yin, Y., Li, B., Liu, G., and Cai, D. (2013). Hypothalamic programming of systemic ageing involving IKK-β, NF-κB, and GnRH. Nature *497*, 211–216.

Zhang, Y., Kim, M.S., Jia, B., Yan, J., Zuniga-Hertz, J.P., Han, C., and Cai, D. (2017). Hypothalamic stem cells control ageing speed partly through exosomal miRNAs. Nature *548*, 52–57.

## STAR★METHODS

### KEY RESOURCES TABLE

| REAGENT or RESOURCE | SOURCE | IDENTIFIER |
|---|---|---|
| Antibodies | | |
| NAMPT polyclonal antibody | Bethyl | A300-372A |
| NAMPT monoclonal antibody | Adipogen | OMNI379 |
| GAPDH | Millipore | MAB374 |
| CD63 | Santa Cruz | sc-5275 |
| Alix | Santa Cruz | Sc-53540 |
| CD81 | Santa Cruz | Sc-166029 |
| CD9 | BD Pharmingen | 553758 |
| TSG101 | Abcam | ab125011 |
| Albumin | Abcam | Ab137885 |
| Transferrin | Abcam | ab82411 |
| Adiponectin | Abcam | Ab22554 |
| Mouse Complement Factor D/Adipsin | R&D systems | MAB5430 |
| Chemicals, Peptides, and Recombinant Proteins | | |
| Dextrose | Hospira, Inc | Cat# 0409-6648-02 |
| Insulin | Eli Lilly | NDC 0002-8215-01 |
| Proteinase K | Sigma | Cat# P2308 |
| Poly-L-lysine | Sigma-Aldrich | Cat# P9155 |
| AraC | Sigma | Cat# C6645 |
| DNaseI | Sigma | Cat# DN25 |
| Opti-MEM | GIBCO | Cat# 31985 |
| BODIPY TR ceramide | Thermo Fisher | Cat# D7540 |
| shNAMPT lentivirus particle | Sigma | TRCN0000101276 |
| Critical Commercial Assays | | |
| RNeasy Mini Kit | QIAGEN | Cat# 74104 |
| High-Capacity cDNA Reverse Transcription Kit | Thermo Fisher | Cat# 4368814 |
| Total Exosome Isolation Kit (from plasma) | Thermo Fisher | Cat# 4484450 |
| Exosome Spin Column | Thermo Fisher | Cat# 4484449 |
| His-3xFlag-NAMPT | N/A | N/A |
| Experimental Models: Cell Lines | | |
| Cell line: HEK293 | ATCC | CRL-3216 |
| Cell line: OP9 | ATCC | CRL-2749 |
| Experimental Models: Organisms/Strains | | |
| Mouse: C57BL/6J | The Jackson Laboratory | RRID: IMSR_JAX:000664 |
| Mouse: Aged C57BL/6J | NIA aging colony | N/A |
| Mouse: ANKI | N/A | N/A |
| Software and Algorithms | | |
| Prism 5 | GraphPad | www.graphpad.com |

### CONTACT FOR REAGENT AND RESOURCE SHARING

Further information and requests for resources and reagents should be directed to the Lead Contact, Shin-ichiro Imai (imaishin@wustl.edu).

## EXPERIMENTAL MODEL AND SUBJECT DETAILS

### Animal Models

All mouse experiments and procedures were approved by the Institutional Animal Care and Use Committee (IACUC) at Washington University in St. Louis and were in accordance with NIH guidelines. C57BL/6J mice were bred in our laboratory using mice purchased from Jackson Laboratories or obtained from the NIH aged rodent colony. Young (4-6 month-old) and aged (18-26 month-old) mice used in each experiment were age- and source-matched. Cre-inducible STOP-*Nampt* mice and adiponectin-Cre mice were generously provided by Joseph Baur at University of Pennsylvania and Evan Rosen at Beth Israel Deaconess Medical Center, respectively. All lines were backcrossed to the C57BL/6J background. For the entire study, heterozygous ANKI mice were generated by crossing heterozygous Adiponectin-Cre mice and homozygous STOP-*Nampt* mice. Both male and female ANKI mice were used for their characterizations including eNAMPT and tissue $NAD^+$ quantifications, wheel-running analysis, sleep fragmentation counts, ERG analysis, and lifespan. Only male ANKI mice were used for gluco-metabolic and islet morphometric analyses due to their more robust phenotypes. All mice were fed a standard chow diet (LabDiet 5053; LabDiet, St. Louis, MO) *ad libitum* and housed at 22°C on a 12/12-hour light/dark cycle in a group of 4-5 unless noted otherwise. Cages and beddings were changed once per week. Mice were monitored periodically for their health status, and there were no viral and parasitic infections during our study.

### Human Subjects

Human plasma samples used for eNAMPT quantification were obtained from male subjects with age ranging from 37 to 80 at Washington University in St. Louis. Individual ages of each patient are shown on the figure. Because no detailed clinical information was collected at the time of sample collection, such information cannot be reported here. The protocol for obtaining plasma and its use in research was reviewed and approved by the Human Research Protection Office of Washington University in St. Louis. Signed informed consents were obtained from all subjects prior to blood collection.

### Cell Culture

HEK293 were obtained from ATCC (Manassas, VA) and maintained in DMEM (Sigma Aldrich, St. Louis, MO) supplemented with 10% FBS, 100U/ml penicillin, and 100μg/ml streptomycin. OP9 preadipocytes were maintained in α-MEM (Sigma Aldrich, St. Louis, MO) supplemented with 20% FBS and penicillin-streptomycin. All cells were maintained at 37°C and 5% $CO_2$. OP9 preadipocytes were differentiated into fully differentiated adipocytes by culturing in α-MEM with 0.2% FBS, 175 nM insulin, 900 μM oleate bound to albumin for 48 hrs. Primary hypothalamic neurons were isolated from E14 embryo and cultured in neurobasal media (Sigma Aldrich, St. Louis, MO) supplemented with 10% FBS, 2mM L-glutamate, and B27. HEK293 was derived from a female fetus. The sex of a mouse from which OP9 preadipocytes were derived is not known. Primary hypothalamic neurons were isolated from both sexes of embryos.

## METHOD DETAILS

### Lifespan and Hazard Rate Analyses

All animals were kept in our animal facility with unlimited access to standard laboratory diet and water. Mice set aside for the survival study were not used for any other biochemical, physiological, or metabolic analyses. All mice in the aging cohorts were carefully inspected daily. The endpoint of life was determined when each mouse was either found dead or euthanized according to our IACUC guidelines. Necropsy was conducted immediately following the death or euthanasia by the Washington University Mouse Pathology Core. Age-associated mortality rate ($q_x$) was calculated by the number of animals alive at the end of each interval over the number of animals at the beginning of the interval. The hazard rate ($hz$) was calculated by $hz = 2\,q_x/(2 - q_x)$, and natural logarithm of $hz$ was plotted against time.

### Physical Activity

Assessment of locomotor activity was performed at the Washington University Animal Behavior Core. Briefly, individual mice were placed into a transparent polystyrene container surrounded by pairs of 4x8 matrix of photocells which quantified total number of ambulation. Another sets of photocells were located 7 cm above the floor to quantify vertical rearing motion. Assessment of wheel-running activity was performed by placing mice in individual cages with a running wheel and housed in circadian cabinetry under 12:12 light-dark cycle. Mice were habituated for 2 weeks before wheel-running activity measurements.

### Sleep Analysis

Mice are anesthetized with isofluorane and surgically implanted with screw electrodes in the skull for electroencephalography (EEG) and stainless wire electrodes in the nuchal muscle for electromyography (EMG). Mice were recovered from surgery for three days and subsequently habituated in the recording cage for two weeks. EEG/EMG recording was performed continuously for 2 consecutive days. 10-second epochs of EEG/EMG signals were visually scored as wake [low amplitude delta (1-4Hz) and theta (4-8Hz) frequency with high EMG activity], NREM sleep [high amplitude delta in the absence of EMG activity], and REM sleep [low amplitude rhythmic theta activity in the absence of EMG activity]. Scorer was blinded for genotypes during quantification.

### Metabolic Assessments

For glucose tolerance tests, mice were intraperitoneally injected with one dose of dextrose (1g/kg body weight) after overnight fasting in aspen bedding. Blood was collected from the tail vein at each time point for the measurement of blood glucose and insulin levels. For insulin tolerance tests, mice were intraperitoneally injected with insulin (0.70 units/kg body weight), and blood was collected from tail vein for the measurement of blood glucose. Quantification of plasma insulin levels was performed using the Singulex assay at the Core Laboratory for Clinical Studies at Washington University. EchoMRI was performed at the Diabetes Models Phenotyping Core of the Diabetes Research Center at Washington University.

### Electroretinography

Mice anesthetized by a mixture of ketamine and xylazine were subjected to ERG using UTAS-E3000 Visual Electrodiagnostic System. Quantitation of ERG waveforms were performed using an existing Microsoft Excel macro that defines a-wave amplitude as the difference between the average baseline and the most negative point of the average trace and also defines b-wave amplitude as the difference between the most negative point to the highest positive point of the wave peak.

### Small Cohort Prospective Lifespan Analysis

Female C57BL/6J mice at 26-28 months of age were obtained from the NIA aging colony. Plasma was collected from the tail vein blood to quantify eNAMPT levels. Subsequently, the mice were housed in groups of 4 mice per cage and untouched except for daily inspection. The number of days from the blood collection to the death was calculated as a remaining lifespan.

### Western Blot Analysis of eNAMPT

Plasma was collected from the tail vein by capillary or cardiac puncture with syringe pre-treated with heparin sulfate under ketamine-xylazine anesthetization. Blood was span down at 3000 x g. 2 μl of freshly collected plasma was incubated with 200 μl of 1x sample buffer at 95°C for 10 min before being stored at -30°C until its use. Right before the analysis, 5μl of each sample was added to 45μl of 1x sample buffer and further incubated at 95°C for 30min. This 30-min boiling was necessary to make eNAMPT bands discrete and quantifiable. Plasma eNAMPT was detected as doublets when the run time of SDS-PAGE was long enough. 10 μl of the final mixture was separated on 4-15 % SDS-PAGE and analyzed by Western blotting with anti-NAMPT polyclonal antibody (Bethyl) for mice and anti-NAMPT monoclonal antibody (Adipogen) for humans. NAMPT antibodies were used at 1:1000 dilutions. All other antibodies were used at 1:100 dilutions.

### Gene Expression Analysis

RNA was extracted by RNeasy Mini Kit (QIAGEN) and converted to cDNA by High-Capacity cDNA Reverse Transcription Kit (Thermo). Quantitative real-time RT-PCR was conducted with the StepOnePlus system (Applied Biosystems), and relative expression levels were calculated for each gene by normalizing to *Gapdh* levels and then to the average of the control mice.

### EV Purification and Characterization

EVs used in this study were isolated using ultracentrifugation or the Total Exosome Isolation Kit From Plasma (ThermoFisher Scientific) according to the manufacturer's instruction. Mouse plasma was isolated by centrifuging blood at 1,000 x g for 10 min. EVs were also collected *in vitro* by conditioning serum free α-MEM with fully differentiated OP9 adipocytes for 48 hrs. Isolated plasma and OP9 conditioned media were centrifuged at 1000 x g for 10 min. Supernatant was centrifuged again for 2000 x g for 20 min. The resulting supernatant was further centrifuged at 10,000 x g for 30 min prior to EV isolation.

For EV isolation from plasma by ultracentrifugation, plasma was diluted 1:1 in PBS and centrifuged at 100,000 x g for 2 hrs. The resulting supernatant was collected for western blot analysis and remaining pellet was resuspended into the volume of PBS equal to the starting plasma volume and centrifuged again at 1000,000 x g for 2 hrs. For EV isolation from OP9 conditioned media by ultracentrifugation, media was centrifuged at 100,000 x g for 2 hrs. Again, resulting supernatant was collected for western blot analysis, and the remaining pellet was resuspended into the volume of PBS equal to the starting volume of media. Resuspended EVs were centrifuged again at 100,000 x g for 2 hrs. The final resulting pellet of EVs from both plasma and OP9 conditioned media was resuspended in 50 μl of PBS.

For EV isolation by the Total Exosome Isolation (TEI) kit, EVs were resuspended in the same volume of PBS as the volume of plasma used to isolate EVs unless noted otherwise. The resulting supernatant subsequent to EV isolation was collected as the soluble protein fraction. The quality of isolated EVs was confirmed by measuring the levels of EV marker proteins [Alix (Santa Cruz Biotechnology), TSG101 (Santa Cruz Biotechnology), CD63 (Santa Cruz Biotechnology), CD81 (Santa Cruz Biotechnology) and CD9 (BD Bioscience)], and non-EV proteins [transferrin (abcam), albumin (abcam), adiponectin (abcam), and adipsin (R&D)]. 40 μg of protein from total plasma, isolated EV fraction, and supernatant/soluble protein fraction were loaded to a SDS-PAGE gel and evaluated by Western blotting.

### Sucrose Gradient Fractionation Analysis of EVs

EVs were prepared by either ultracentrifugation at 100,000 x g for 2 hrs or by the TEI kit. The isolated EVs were diluted with 90% sucrose solution to a final concentration of 82%. The EVs were then layered at the bottom, and subsequently, sucrose solutions

ranging from 82%-10% were layered above. Samples were centrifuged at 100,000 x g for 20 hrs, and 6 fractions were collected. Each fraction was diluted 1:100 in PBS and centrifuged at 100,000 x g for 2 hrs to pellet EVs. A pellet from each fraction was then resuspended in an equal volume of PBS and subjected to the analysis by Western blotting.

### Proteinase K Digestion Assay

Proteinase K was added to 50 μl of plasma at the final concentration of 1 μg/μl and incubated at 37°C for 10 min. Subsequently, 25 μl of PBS and 15 μl of the Exosome Precipitation Reagent (ThermoFisher Scientific) were added, and the mixture was incubated on ice for 30min. The mixture was centrifuged at 1000 x g, and the precipitated EVs were analyzed by Western blotting.

### Proteomic Analysis of Plasma EVs

Plasma was isolated from EDTA-supplemented blood isolated from 6 and 24 month-old wild-type B6 female mice and 24 month-old control and ANKI female mice. EVs were isolated from 400 μl of plasma by ultracentrifugation and reconstituted in water. Proteins were extracted and analyzed by Progenesis LC-MS (NonLinear Dynamics). Protein identification was done with Mascot Server v2.4 (Matric Science). A list of identified proteins was generated with peptide threshold with 95% minimum, protein threshold with 95% minimum and 2 peptides minimum, and protein false discovery rate at 0.5%. Out of 248 proteins identified with above threshold, 181 proteins were identified in the past proteomic study of EVs/exosomes, based on EVpedi.org and were used to generate the heatmap.

### Isolation of Primary Hypothalamic Neurons

Hypothalami from E16-E18 embryos were dissected and placed on ice in the Hibernate E medium. Hypothalami were digested in 0.25% trypsin-EDTA (Sigma) supplemented with DNase I (Sigma) at 37°C for 15 min. After an equal volume of DMEM supplemented with 10% FBS was added, cells were gently dissociated by pipetting until no clumps remained. Cells were collected by centrifuging at 450 x g for 5 min at room temperature. Cells were washed and resuspended in the Neurobasal media containing 10% FBS, 2% B27, 2M L-glutamine, and antibiotics. Cells were plated onto wells directly or onto coverslips pre-coated with poly-l-lysine (Sigma). Two days after the isolation, cells were treated with 10μM Ara-C (Sigma) for at least 4 days or until non-neural cells were eliminated.

### EV Internalization Assay

Isolated EVs were resuspended in PBS. BODIPY TR ceramide in DMSO was added to EVs or PBS at the final concentration of 100 μM and incubated at 37°C for 1 hr. Unincorporated dye from the labeled EVs was removed by Exosome Spin Column (ThermoFisher Scientific) following manufacturer's instructions. Purified EVs or PBS solution was added directly to primary hypothalamic neurons growing on coverslips and incubated for 30 min. Following incubation, cells were washed in PBS and fixed in 4% paraformaldehyde.

### Generation of Recombinant NAMPT-Containing EVs and Their Internalization Assay

Isolated EVs were resuspended in 1μg/μl FLAG-tagged recombinant NAMPT protein (recNAMPT) and incubated overnight at 37°C. recNAMPT-containing EVs were isolated from the mixture by adding 0.2 volume of Exosome Precipitation Reagent (ThermoFisher Scientific). recNAMPT-containing EVs were reconstituted into the same volume of PBS as that of the starting plasma.

### Wheel-Running Assay after EV Injection

For EV injection experiments, 20-month-old male and female mice were habituated by 6 days of mock injection. For pre-treatment measurements of wheel-running activity, mice were intraperitoneally injected with 100 μl of PBS for 4 days. Subsequently, the same mice were injected with 100 μl of resuspended EVs purified from 200 μl plasma collected from 4-6 month-old mice and resuspended in PBS. Every injection was performed approximately at 5:30pm.

### Lifespan Study of EV-Injected Mice

25-month-old female C57BL/6J mice were obtained from the National Institute on Aging (NIA). Mice were sorted by their weights, and pairs of mice with similar body weight were allocated to each group. Four mice were housed per cage. EVs were isolated from plasma of 4–12-month-old wild-type mice by the TEI kit. In this lifespan study, the use of the TEI kit was necessary to achieve the highest yields of EVs from the limited numbers of available mice. EVs isolated from 500 μl of plasma were resuspended in 100 μl of PBS and administered to mice once a week by intraperitoneal injection, starting at 26 months of age.

## QUANTIFICATION AND STATISTICAL ANALYSIS

### Data Analysis

Results are presented as mean ± SEM. All statistical tests were performed using GraphPad Prism 5. Significance between two groups was assessed by Student's *t* test. Normality of the data was assessed graphically. The comparisons between multiple groups

were carried out using one-way ANOVA with Tukey posthoc test. Analysis of plasma eNAMPT levels over 24 hrs between 6 and 18 month-old mice was performed using two-way repeated measures ANOVA. Linear regression analysis was used to analyze plasma eNAMPT levels of mice and humans across different age groups. Comparison of locomotor and wheel-running activities was performed by Wilcoxon matched-pairs singled-ranked test. ERG signal was analyzed by two-way repeated measures ANOVA with Bonferroni *posthoc* test. Gehan-Breslow-Wilcoxon test was used for the statistical analysis of lifespan. Fisher's exact test was used to compare the proportion of the cause of death. Statistical comparison of wheel-running activities in pre- and post-treatments with EV injection was performed by a paired *t* test. Sample sizes and other statistical parameters are indicated in the figures and texts. *$p< 0.05$, **$p< 0.01$, ***$p< 0.001$. Significance was concluded at $p< 0.05$.